HOKKAIDO UNIVERSITY

Title	Dissolved iron distribution in the western and central subarctic Pacific : HNLC water formation and biogeochemical processes
Author(s)	Nishioka, Jun; Obata, Hajime
Citation	Limnology and Oceanography, 62(5), 2004-2022 https://doi.org/10.1002/lno.10548
Issue Date	2017-04-06
Doc URL	https://hdl.handle.net/2115/68796
Rights	This is the peer reviewed version of the following article: Limnol. Oceanogr. 62, 2017, 2004-2022, which has been published in final form at [doi: 10.1002/lno.10548]. This article may be used for non-commercial purposes in accordance with Wiley Terms and Conditions for Self-Archiving.
Type	journal article
File Information	Nishioka and Obata 2017.pdf

Hokkaido University Collection of Scholarly and Academic Papers : HUSCAP

Dissolved iron distribution in the western and central subarctic Pacific - HNLC water formation and biogeochemical processes -

Jun Nishioka[1)], Hajime Obata[2)]

1) Institute of Low Temperature Science, Hokkaido University, N19W8, Sapporo, Hokkaido 060-0819, Japan,

2) Atmosphere and Ocean Research Institute, The University of Tokyo, Kashiwa, Chiba 277-8564, Japan

Keywords: Japan-GEOTRACES, iron, subarctic Pacific

CORRESPONDENCE and requests for material to:
Jun Nishioka,
Institute of Low Temperature Science, Hokkaido University,
19NW8, Kita-ku, Sapporo, Hokkaido 060-0819, Japan
Tel: +81-11-706-7655, Fax: +81-11-706-7655
E-mail: nishioka@lowtem.hokudai.ac.jp

Abstract

It is well known that phytoplankton growth is broadly limited by iron (Fe) availability in the subarctic Pacific. To investigate which Fe sources control the amplitude of seasonal variation in biogeochemical parameters in the subarctic Pacific, we examined the spatial variation in the west-to-east distribution of dissolved Fe (DFe) across the western and central subarctic Pacific through the Japanese GEOTRACES program. The vertical section profile of the western subarctic Pacific gyre showed high dissolved Fe concentrations from the bottom of the surface mixed layer to as deep as approximately 3000 m, suggesting that Fe-rich intermediate water is transported laterally and distributed across the western subarctic gyre, over 2000 km. The section data also indicate that the influence of the western Fe-rich intermediate water does not reach the Alaskan gyre. Fe* index (= [DFe] (observed) – [PO_4] (observed) × RFe:P) distribution clearly indicates that the western Fe-rich intermediate water is well explained by external sedimentary Fe sources and water transport systems from a subpolar marginal sea, the Sea of Okhotsk, and the continental margin. The spatial pattern of Fe to nutrient stoichiometry supplied from the intermediate water to the surface, in comparison with reported Fe and nutrient demand in surface phytoplankton, quantitatively explains the differences in surface macronutrient consumption between the western and eastern gyre as well as the formation of the high nutrient and low chlorophyll region in the whole subarctic Pacific.

Iron (Fe) is an essential nutrient that plays an important role in the control of phytoplankton growth and ocean biogeochemistry (Martin et al. 1989). Atmospheric dust, which has been well studied, was once thought to be the major source of Fe in many oceanic regions (e.g., Duce and Tindale 1991; Jickells et al. 2005; Grand et al. 2015). Other sources of Fe in ocean basins such as sedimentary, hydrothermal, volcanic, and sea ice- and iceberg-derived Fe have since been identified (e.g., Johnson et al. 1999; Measures 1999; Elrod et al. 2004, 2008; Lam et al. 2006, 2012; Smith et al. 2007; Aguilar-Islas et al. 2007; Nishioka et al. 2007, 2013a; Wu et al. 2009; Hurst et al. 2010; Boyd and Ellwood 2010; Tagliabue et al. 2014a), and recently international GEOTRACES studies have revealed the global importance of these Fe sources (e.g., Nishioka et al. 2013b; Conway and John 2014; Rijkenberg et al. 2014; Hatta et al. 2015; Resing et al. 2015).

The subarctic Pacific is known to be a high-nutrient, low-chlorophyll (HNLC) region, where macronutrient concentrations do not become depleted throughout the year and phytoplankton growth is broadly limited by Fe availability (e.g. Martin and Fitzwater 1988). Sedimentary Fe, in particular, has been shown as an important Fe source in the subarctic Pacific (Lam et al. 2006; Nishioka et al. 2007, 2013a; Tagliabue et al. 2014b). Sedimentary resuspension enriches Fe in the bottom water above the continental shelves, located around the margins of the Pacific basin and in its marginal seas (e.g., Elrod et al. 2004; Lohan and Bruland 2008; Hurst et al. 2010; Nishioka et al. 2013a). Previously, it was thought that the effect of sedimentary Fe was mostly local, but it has recently been demonstrated that sedimentary DFe can be transported for longer distances than that had been thought and can thus be dispersed throughout entire ocean basins (Nishioka et al. 2007; 2013a; Lam and Bishop 2008). Additional evidence

of the long-distance transport of sedimentary Fe has been provided by Conway and John (2015) in a recent Fe isotope study that water enriched in sedimentary Fe is likely transported across the Pacific via North Pacific Intermediate Water (NPIW).

Two cyclonic gyres dominate circulation in the subarctic Pacific: the western subarctic gyre (WSG) west of 175°E, and the Alaska gyre (AG) east of 165°W, with the central subarctic North Pacific (CNP) in the middle (delineated in Fig. 1). Seasonal variation in biogeochemical parameters has historically been greater in the WSG than in the AG (Shiomoto et al. 1998; Shiomoto and Asami 1999; Harrison et al. 1999, 2004), even though both water masses have HNLC characteristics. Time series studies in both gyres, station KNOT and K2 for WSG and Station P for AG (e. g. Whitney and Freeland 1999; Tsurushima et al. 2002; Fujiki et al., 2014), and basin-scale data-mapping analyses (Whitney 2011; Yasunaka et al. 2014) have shown that higher nutrient concentrations accumulate in the surface water of the WSG in winter, compared with in the AG, and the nitrate drawdown from spring to summer in the Oyashio-Kuroshio transition zone (OKTZ) and in the WSG is double that in the AG (Yasunaka et al. 2014). Moreover, the seasonal amplitude of the biological drawdown effect on pCO_2 in the surface water is higher in the OKTZ and in the WSG than in the AG (Takahashi et al. 2002; Chierici et al. 2006). Suzuki et al. (2002) and Fujiki et al. (2014) have reported that the photochemical quantum yield (*Fv/Fm*), which quantifies the efficiency of photosynthesis and often responds to Fe supply, is significantly higher in the WSG than that in the AG. Spring phytoplankton growth in the WSG (Shiomoto et al. 1998; Imai et al. 2002; Isada et al. 2010), which consists mainly of diatoms (Mochizuki et al. 2002), leads to extensive transport of organic carbon to the deep ocean (Buesseler et al. 2007; Honda 2003; Kawakami et al. 2015), causing the drawdown of nutrients and

94 pCO_2. The various biogeochemical differences between these two gyres are summarized
95 in Table 1.
96 In HNLC waters, differences in Fe supply processes are critical to understanding
97 the differences in seasonal phytoplankton growth and in the amplitude of the seasonal
98 variation in biogeochemical parameters observed between the WSG and the AG.
99 Nishioka et al. (2013a) obtained a detailed basin-wide meridional DFe section along
100 155°E from the Sea of Okhotsk (a northern marginal sea) to the subtropical gyre,
101 including the WSG, and demonstrated that the intermediate water mass of the WSG is
102 enriched in Fe by sedimentary Fe supplied from the Sea of Okhotsk. They also showed
103 that the Fe-rich intermediate water in the WSG has a higher ratio of DFe to
104 macronutrients than the intermediate water in the AG. They concluded that the existence
105 of Fe-rich intermediate water is probably a key determinant of water characteristics in
106 the WSG (Nishioka et al. 2013a). Therefore, a more detailed knowledge of the
107 distribution of the Fe-rich intermediate water would improve our understanding of the
108 whole subarctic Pacific biogeochemical system. Although several previous studies have
109 shown that there is a west–east gradient in the DFe concentration in the subarctic water
110 column (Nishioka et al. 2003, 2013a; Kitayama et al. 2009; Uchida et al. 2012),
111 observations of DFe concentrations are still too scarce for us to fully characterize the
112 west-to-east Fe distribution in the subarctic Pacific.
113 In this study, we present a new extensive west–east zonal section full depth
114 transect of DFe across the western and central subarctic Pacific obtained during the
115 Japanese GEOTRACES program. Several vertical profiles of total dissolvable Fe are
116 also presented. We then compare the section profile in the western and central subarctic
117 Pacific with the previously reported section profile in the AG and discuss the detailed

118 spatial distribution and sources of DFe that control the magnitude of biogeochemical
119 variation and the HNLC water formation in the subarctic Pacific.
120

121 ***Methods***

122 **Vertical section observations**

123 The KH-12-4 cruise of R/V *Hakuho-maru* (coordinated by the Japanese
124 GEOTRACES program (GP 02)) made zonal vertical section observations from west to
125 east across the subarctic Pacific (around 47°N; Fig. 1) from August to October 2012.
126 Although the transect extended from Japan to the western coast of Canada in the initial
127 plan, we were unfortunately unable to carry out observations at several stations in the
128 AG because of stormy weather conditions. Data obtained near the western coast of
129 Canada, in the vicinity of the Juan de Fuca hydrothermal vent, will be reported
130 elsewhere. Thus, in this report, we examine 13 full-depth vertical profiles that together
131 form a vertical section profile across the western and central subarctic Pacific (BD 4–
132 BD 16; Fig. 1).

133 To obtain the full depth vertical profiles of DFe, we conducted sampling and
134 sub-sampling in accordance with the GEOTRACES protocol as described by Nishioka
135 at al. (2013b). Hydrographic data and seawater samples were collected using a clean
136 conductivity-temperature-depth (CTD)-carousel multiple sampler system (CMS, SBE-
137 911plus and SBE-32 water samplers, Sea Bird Electronics, Inc.), connected via a
138 titanium armored cable, on which 24 acid-cleaned Teflon-coated 12-L Niskin-X bottles
139 were mounted. At station BD 8, seawater samples from the upper layers (10 to 200 m)

were collected using a Niskin-X sampler attached directly to a titanium hydro-wire equipped in *R/V Hakuho-maru* because stormy weather did not permit us to deploy the CTD system for the shallow casts. Using both methods, we could obtain the identical waters for determination of Fe and Zn (Kim et al. 2015). To sub-sample from the Niskin-X samplers, they were taken in a clean air bubble (filled with air that had been passed through a HEPA filter). We connected a 0.2 μm Acropak filter (Pall Corporation) to the Niskin-X spigot and added a pressure of 1 atm to the Niskin-X samplers by compressed clean air; then, the filtrate was collected in acid-cleaned 125-mL LDPE bottles (Nalgene Co., Ltd).

The filtrate (<0.2 μm) was adjusted to pH < 2 by the addition of ultrapure HCl (Tamapure AA-10, the final concentration to be 0.05 M) and then allowed to stand for approximately 24 h at room temperature in the onboard clean room. It was then adjusted to pH 3.2 just before the sample measurements by the addition of ammonium solution and a formic acid (10 M)–ammonium (2.4 M) buffer. Then, DFe, defined as the leachable Fe in the filtrate at pH < 2, was analyzed onboard by using a flow-injection analysis (FIA) chemiluminescence detection system (Obata et al. 1993, 1997). Unfiltered samples collected from several stations (BD 7, BD 9, BD 11, BD 14, BD 15) were adjusted to pH < 2 onboard and stored for several months at room temperature; then, in the onshore laboratory, the pH was readjusted to 3.2 (as described above for DFe) immediately before the samples were analyzed for total dissolvable Fe, defined as dissolved Fe plus leachable particulate Fe in the unfiltered samples at pH < 2, with the FIA chemiluminescence detection system (Obata et al. 1993, 1997). All sample treatments were performed under laminar flow in the onboard or onshore clean-air laboratory.

The DFe measurements and the reference seawater used in this study were quality controlled by using SAFe (Sampling and Analysis of Iron) cruise (Johnson et al. 2007) reference standard seawater (obtained from the University of California Santa Cruz for an inter-comparison study). We measured a SAFe reference sample during every sample measurement run of the FIA instrument performed in the onboard and onshore laboratories. The consensus values for Fe (III) in the SAFe reference standard seawater are 0.093 ± 0.008 nM (S) and 0.933 ± 0.023 nM (D2) (May 2013, www.geotraces.org), and we obtained values of 0.091 ± 0.0128 nM (n = 26) (S) and 0.963 ± 0.083 nM (n = 22) (D2) by our method. This good agreement demonstrates that our data quality was high and that our data are comparable with the global GEOTRACES dataset. The detection limit (three times the standard deviation of the Fe (III) concentration (0.036 nM) of purified seawater that had been passed through an 8-quinolinol resin column three times to remove Fe) was 0.020 nM.

Nutrient concentrations were also measured at the same stations. Unfiltered seawater samples were collected in 15 ml acrylic tube and nutrients (nitrate+nitrite (hereafter N+N), phosphate, silicate) concentrations were measured onboard with a SWAAT auto-analyzer (BL-TEC Japan) immediately after sampling. This measurement was quality controlled by using the reference material (RM; KANSO, Lot No. AV), and we obtained the values consistent with consensus values for nitrate+nitrite (33.21 μM), phosphate (2.48 μM), and silicate (156.6 μM). Detection limits for the measurement were 0.03 μM for N+N, 0.01 μM for phosphate, and 0.08 μM for silicate. Vertical profiles of our nutrients data (BD 7) were well consistent with WOCE data profiles which had been obtained at the same location (Kim et al, submitted). Hydrographic data were also collected at all stations by the CTD sensor.

188 Dissolved oxygen (DO) was measured with an SBE-43 sensor (Sea Bird Electronics,
189 Inc.) mounted on the CTD frame, and the data were calibrated by onboard
190 measurements of discrete vertical samples by the Winkler method.

191

192 ***Results***

193 **Hydrography and water definition**

194 Vertical section profiles of temperature, salinity, and DO in the western and central
195 subarctic Pacific are presented in Fig. 2a–c. In this study we define the area according to
196 Kim et al. (Submitted). Here the definition of the area is outlined. At BD 4, warm-high
197 salinity Kuroshio water affected surface layer (Fig. 2 a, b). At BD 5, surface water has
198 slightly higher temperature and salinity than subarctic water which existed below the
199 surface. These results indicate that BD 4 and BD 5 was located in the OKTZ (from
200 143°54'E to 150°E).

201 As described briefly above, the subarctic Pacific consists of the WSG and the AG.
202 The WSG is composed of the East Kamchatka Current, the Oyashio Current and the
203 Subarctic Current (Fig. 1), and is strong influenced by waters which are discharged from
204 the Bering Sea and the Okhotsk Sea. Judging from obtained water properties, specifically
205 relatively cold shallow waters, we defined that BD 6, BD 7, BD 8, BD 9 are located in
206 the WSG (from 155°E to 170°35'E).

207 The AG is formed by the westward Alaskan Stream (AS) which recirculates near
208 170° W into the eastward Subarctic Current (Bograd et al., 1999) (Fig. 1). Judging from

209 slightly warmer and lower salinity surface water than WSG, we define BD 15 and BD 16
210 as located in the AG (eastern from 160°'W). Those gyres are connected by the eastward
211 Subarctic Current and westward AS (Fig. 1). This area is defined as central subarctic
212 north Pacific (CNP), which has relatively warmer surface water than the WSG, indicating
213 influence of mixed water of Kuroshio and Oyashio water transported by the eastward
214 Subarctic Current. In our section, BD 11, BD 13, BD 14 were located in the CNP area
215 (from 180°E to 170°W).

216 In this study, intermediate water mass is defined as 26.6-27.5σ_θ density range (Fig. 2
217 c). It has been revealed that the water in this density range in the subarctic Pacific is
218 strongly influenced by water from the East Kamuchatka Current and the Okhotsk Sea
219 water, and is a source water for the formation of the NPIW which expands to subtropical
220 areas. Although surface waters at BD 4 were influenced by subtropical Kuroshio water,
221 there were salinity minimum at 26.8 σ_θ isopycnal depth which indicate the water mass of
222 the NPIW intruding under the Kuroshio influenced water mass (Yasuda et al. 2004). In
223 the subarctic Pacific, several studies have reported that biogeochemical signals from the
224 NPIW source region (including marginal seas), such as decreasing trend of oxygen
225 concentration, are propagated from west to east in this intermediate water density range
226 (Emerson et al. 2004; Nakanowatari et al. 2007; Watanabe et al. 2008; Uehara et al.
227 2014).

228

229 **Nutrient distribution**

230 Surface waters concentrations of N+N and silicate are presented in Fig. 3a. Nutrient

(N+N, phosphate and silicate) vertical section profiles (including all stations along the section except BD 10 and BD 12) are presented in Fig. 4a, 4b and 4c. Surface N+N concentration was depleted at BD 4 and BD 5, which are defined as the OKTZ. Residual surface N+N and silicate in the WSG exceeded ~10 μM, respectively, from BD 6 (155°E) eastward (Fig. 3a). In the section profiles, maximum N+N (Fig. 4a) and phosphate (Fig. 4b), and minimum DO (Fig. 2c) concentrations were observed in the intermediate layer (26.8-27.0 σ_θ density range). The distribution of silicate was similar to that of N+N in the surface layer, but the highest silicate concentrations extended to greater depths (Fig. 4c), indicating that the silica regeneration depth was different from that of N+N, as has been observed in the literature globally (Sarmiento and Gruber, 2006). In deep water (below 4000 m), the silicate concentration showed a clear eastward-increasing gradient, but the N+N and phosphate concentration did not show this same gradient.

Dissolved Fe distribution

Vertical DFe profiles in all stations show a nutrient-type distribution, depleted at the surface with elevated levels with increasing depth (Fig. 5). The average surface DFe concentrations at 10 m and 25 m depth at stations along the section (BD 4–16) ranged from 0.05 to 0.20 nM (Fig. 3b). Relatively higher concentrations were observed at BD 4 and BD 12 (Fig. 3b), where the Kuroshio water and the AS influence is found (Fig. 1). In the section profile (Fig. 6a, including all stations except BD 10 and BD 12), intermediate waters (500–2500 m) from BD 4 to BD 9, DFe concentrations were markedly higher in the OKTZ and WSG (~1.8 nM) than in the CNP and AG (~ 0.9 nM), indicating an extension of Fe enrichment from lateral sources for more than 2000 km eastward across the subarctic

Pacific. In this region, lateral sources of Fe might play a role in creating these high concentrations, as discussed later.

In the section profile, DFe concentrations were low (<0.5 nM) below 4000 m depth from BD 4 to BD 9 and below 2500 m depth eastward from BD 11 to BD 16 (Fig. 6a). At BD 16, the concentration range of DFe in deep water (~ 0.6 nM) was similar to that at ocean station Papa (T7 in Fig. 1; ~ 0.7 nM), reported by Martin et al. (1989).

Discussion

Surface dissolved Fe distributions

Surface N+N and silicate were not depleted at the stations from BD 6 (155°E) eastward to at least BD 16 (156°W) (Fig. 3a). This result is consistent with previous findings that a wide area of subarctic waters are characteristically HNLC across the subarctic Pacific from west to east (Whitney and Freeland 1999; Tsurushima et al. 2002; Whitney 2011). Quite low DFe concentrations ranging from 0.05 to 0.12 nM were observed in the surface layer along the section (Fig. 3b), except at the westernmost station (BD 4, 0.2 nM) near the Japanese coast; we could not find clear features of surface elevated Fe concentrations even though high dust levels in the air above the WSG in spring season have been reported (Uematsu et al. 1983; Duce and Tindale 1991; Uematsu et al. 2002) (Fig. 3b). The range of surface DFe values obtained in this study is lower than that reported by Ezoe et al. (2004) at station B001 (39°59'N, 160°E; 0.26–0.51 nM at 0–31 m depth) south of our transect and by Bruland et al (1994) at VERTEX-IV site in the center of North

Pacific subtropical gyre (28°N, 155°W; 0.35~ nM at surface), but comparable to ranges reported previously for the WSG (Nishioka et al. 2003, 2007, 2013a; Brown et al., 2005; Takata et al. 2004). The westernmost station (BD 4) along the transect had a higher surface DFe concentration (~0.2 nM) than the other stations. Both N+N and silicate concentrations were depleted at BD 4, and the N+N concentration was very low at BD 5, at the OKTZ (Fig. 3a), indicating that biological production had consumed the nutrients before our sampling period. Possible sources of the Fe that fueled this biological production are Fe-containing dust, lateral advection of Fe in the surface layer, and an upward supply of Fe from deeper Fe-rich water (discussed later). At all other stations, N+N and silicate concentrations were high in the surface layer (Fig. 3a) and the DFe concentration was very low (Fig. 3b); thus, typical HNLC water was observed along our section across the subarctic Pacific.

Importance of external Fe sources and long range transport in the formation of Fe-rich intermediate water

Although Nishioka et al. (2013a) presented the north–south distribution of DFe from the marginal Sea of Okhotsk through the subarctic region to the subtropical region, the west–east detailed full-depth distribution of DFe has not been previously reported. Our basin-scale zonal high-resolution transect observation provides a comprehensive picture of the DFe distribution in the WSG and surrounding area. The water masses with markedly high DFe concentrations (~1.8 nM) in the intermediate layer were observed in the OKTZ and the WSG (Fig.5 and Fig. 6a) by this study, as seen along the meridional DFe section reported by Nishioka et al. (2013a).

In general, vertical section profiles of DFe reflect the influence of Fe supplied from several potential external sources (hereafter external Fe), such as atmospheric Fe and laterally transported Fe, along with internally recycled Fe (hereafter internal Fe), such as remineralization and release of Fe from organic particles settling in the water column. Therefore, to understand the controlling sources of Fe in the subarctic Pacific, it is necessary to evaluate both external and internal Fe sources. We used the Fe* concept proposed by Parekh et al. (2005) for quantitative evaluation of the spatial pattern of the contributions of internal and external DFe in a section profile. According to Nishioka et al. (2011), we used the following equation, modified from Parekh et al. (2005), to determine Fe*, which we defined as external DFe:

$$Fe^* = \text{external DFe} = [\text{DFe}]\ (\text{observed}) - [PO_4]\ (\text{observed}) \times \text{RFe:P}$$

In this equation, [DFe] and [PO_4] are the observed concentrations in our section profile. Our previous study indicated that PO_4 and DFe are remineralized over similar depth scales in the North Pacific (Nishioka et al., 2011). RFe:P is the ratio of DFe to PO_4 (= 0.26 nM/μM in this study); we derived this value using the intermediate water DFe and PO_4 concentrations at the T7 reported in Martin et al. (1989) in the central AG, where intermediate water may not be strongly influenced by lateral external Fe input. Here, Fe* is defined as DFe supplied external sources decoupled from the phosphate (regeneration) cycle. Therefore, Fe* represents externally supplied DFe, and remineralized DFe from settling organic particles is [DFe] – [Fe*]. We have to be careful that calculated laterally transported DFe is probably underestimated because we did not account for preformed PO_4 which is also laterally transported to the section area

(Kim et al., submitted). In the vertical section profile, Fe* is high in the DFe-rich intermediate water in the OKTZ and the WSG region (Fig. 6b). This result suggests that the Fe-rich intermediate water existing across in the western part of our section is strongly affected by an external Fe supply (decoupled from nutrient cycles). From the Fe* value, it can be estimated that at BD 7 (47°N, 160°E), ~50% of DFe in the Fe-rich intermediate water at 500–2000 m depth was supplied via external Fe sources. High Fe* value is not seen east of 175°E indicating that dilution and/or scavenging processes occur during the Fe transportation. These results suggest that the input of external Fe into the western part of our section is mainly responsible for the differences in the DFe concentration in intermediate waters between the western waters (the OKTZ, the WSG) and the AG. Both the DFe concentration and Fe* value have high peaks at BD 4, BD 5 and BD 7. The high peaks of external DFe are also compatible with previous reports that Fe-rich water is transported from the Sea of Okhotsk (Nishioka et al. 2007, 2013a) and from the continental margin around Kamchatka (Lam and Bishop 2008) to the western part of North Pacific via the intermediate water circulation. This external Fe enrichment of the intermediate water cannot be explained by a surface atmospheric Fe supply, another potential external source of Fe in this region.

At BD 15, the western edge of the AG, the concentration of DFe was higher below the surface layer compared with the surrounding waters, and Fe* was also slightly higher, indicating that the intermediate water at BD 15 was also influenced by external Fe. Previous studies (Martin et al. 1989; Takata et al. 2006; Lam et al. 2006; Lippiatt et al. 2010) have shown that the subsurface water in this region is influenced by water transported by the AS, an offshore current, from the Alaskan margin. Therefore, the higher DFe concentration and Fe* value at BD 15 compared with the

surrounding water probably reflect Fe transported from the Alaskan margin.

Judging from the depth at which we observed high DFe and high Fe*(Fig. 6a and 6b), DFe anomalies in the intermediate layer in the section profile likely reflect the location of the Fe source region (the continental margin/shelf at the edge of the basin and in the marginal seas), the direction of the intermediate water circulation, the strong western boundary current, and long-range lateral transport within the subarctic Pacific.

The ventilation source of the intermediate water in the North Pacific, including the NPIW, which is characterized by a salinity minimum in the subtropical area, is the Sea of Okhotsk (Reid 1965; Yasuda 1997; Talley 2008). This ventilated intermediate water, which has a density of around 26.8 $\sigma_{\theta,}$ is the major intermediate-depth water mass in the whole North Pacific over the OKTZ, the WSG, the CNP and the AG (Reid 1965). As described in the section above, previous studies have suggested that biogeochemical signals are propagated from west to east via the intermediate water (Emerson et al. 2004; Nakanowatari et al. 2007; Watanabe et al. 2008). Additionally, the ventilated intermediate water is influenced by sedimentary Fe input from the Sea of Okhotsk and Kamchatka margin (Nishioka et al. 2007; Lam and Bishop 2008), and the Fe-rich water incorporated in the NPIW influences the meridional Fe section profile (Nishioka et al. 2007, 2013a). Therefore, long-distance lateral transport of DFe from the intermediate water source area is probably key to explaining the section profile of the west-to-east DFe distribution in the subarctic Pacific, as reported in other oceanic areas (e. g. Johnson et al. 1997). These distances of DFe transport in the open-ocean intermediate layer are greater than those predicted by using thermodynamics of DFe in oxic seawater, because the Fe-oxyhydroxides that form in oxic water are subsequently adsorbed onto settling particles

and thus removed from the water column (Lohan and Bruland 2008; Misumi et al. 2011). Further studies of the chemical speciation of Fe, especially organic complexation and/or colloidal particles, in the intermediate water are needed to understand why the DFe in the intermediate water is not efficiently scavenged.

Spatial pattern of Fe to nutrient stoichiometry from sub-surface supply and comparison to Fe and nutrient demand

To explain the difference in amplitude of the seasonal variation in biogeochemical parameters in the two gyres of the subarctic Pacific, both of which have surface HNLC waters, the Fe supply must be higher in the WSG than in the AG, but not high enough for phytoplankton to consume nutrients completely (Nishioka et al. 2013a). Nishioka et al. (2013a) compared a few vertical DFe profiles at representative stations in the WSG and the AG and suggested that the DFe supply from below the surface layer by winter mixing can explain the difference in surface nutrient consumption between the WSG and the AG (twice as high in the WSG as in the AG). By using the section profiles obtained in this study, we are able to evaluate the spatial pattern of Fe supply processes that control the seasonal variation of biogeochemical parameters in the subarctic Pacific.

First, we re-evaluated the upward DFe and N+N fluxes from below the surface. These fluxes can be estimated with the following equations.

$$\text{DFe Flux} = K_\rho \times (d\text{Fe}/dz); \quad (\text{N+N}) \text{ Flux} = K_\rho \times (d\text{N}/dz),$$

where K_ρ is the coefficient of eddy diffusivity. In this study, we try to evaluate DFe flux to N+N fluxes stoichiometry. Therefore, the surface-to-subsurface (bottom of surface mixed layer to maximum concentration depth) gradient of DFe (dFe/dz) and of N+N (dN/dz), and the ratio (dFe/dz)/(dN/dz) at all stations along the section profile were compared to quantitatively evaluate the fluxes stoichiometry (Fig. 7a–c). In this study, we compared the (dFe/dz)/(dN/dz) ratios from our section data with previously published data for line P, which is the section from south Vancouver Island to station P (T7 in Fig. 1) in the AG (Nishioka et al. 2001). In general, the vertical gradient of the DFe increase with depth below the surface was variable among the OKTZ, the WSG, the CNP, the AG, and the AS (Fig. 7a). Interestingly, the subsurface gradient of dFe/dz in the WSG was particularly high (0.0057 μM m^{-4}) at BD 9 (170°35'E), which is the station closest to the Emperor Seamount Chain (Fig. 7a). Although the western edge of AG (BD 15, BD 16) had comparable high gradient values with the WSG (Fig. 7a), the central AG (T7, P20) had lower gradient values than that of the WSG.

The west–east spatial pattern of the subsurface gradient of the N+N concentration (dN/dz) was similar at all stations on the section profiles to the DFe pattern; however, in terms of absolute values, the differences among the stations were not as great as the DFe gradient differences (Fig. 7b). As a result of the gradient differences, the (dFe/dz)/(dN/dz) ratio differed among the waters; the values in the OKTZ (BD 4, BD 5; average 0.039 ± 0.019 nM/μM) were the highest, and the WSG (BD 6, BD 7, BD 8, BD 9; average 0.025 ± 0.008 nM/μM) were significant higher (t-test, 0.05>P) than those of the AG (BD 15, BD 16, T7 and P 20) (average 0.013 ± 0.0047 nM/μM) (Fig. 7c). Although the western edge of the AG (BD15 and BD16) had higher gradient dFe/dz values than the CNP regions (Fig. 7a), the (dFe/dz)/(dN/dz)

417 ratio in these stations do not seem very different from those in the CNP, probably
418 because these stations are influenced by Fe and N+N input via offshore directed
419 currents from the continental margin (Martin et al. 1989; Takata et al. 2006; Lam et al.
420 2006; Wu et al. 2009; Cullen et al. 2009; Lippiatt et al. 2010).

421 Second, to explain the wintertime surface DFe and nutrient supply ratio, we
422 evaluated the spatial pattern of the direct upward transport of DFe and N+N from the
423 intermediate water to the surface via entrainment in wintertime by deep vertical water
424 mixing. The bottom of the winter mixed layer has been well investigated in our studied
425 area, and has been shown to reach the 26.6 σ_θ isopycnal surface in the OKTZ and the
426 WSG, and reach the 26.0 σ_θ surface in the AG (Talley 1991; Suga et al. 2004). It is
427 clear on the west-to-east section profile of the DFe/N+N concentration ratio (nM/μM)
428 in relation to the isopycnal surfaces at the bottom of the winter mixed layer (Fig. 8) that
429 winter surface mixing in the OKTZ (BD 5) and western part of the WSG (BD 6, BD 7)
430 is sufficiently deep to reach the intermediate water, in which the DFe/N+N
431 concentration ratio is >0.015. This ratio is higher than that in the intermediate water of
432 the CNP and the AG (<0.01) (Fig. 8). These results suggest that the DFe/N+N
433 concentration ratio in intermediate water transported to the surface water in the WSG is
434 approximately twice that in the CNP and the AG.

435 The higher values of the DFe to N+N diffusive flux ratio, (dFe/dz)/(dN/dz), and
436 the DFe to N+N concentration ratio in water transported vertically by winter mixing,
437 DFe/N+N, in the WSG compared with those in the AG explain why the nutrient
438 drawdown in the WSG is higher than that in the AG (Table 1). Therefore, the presence
439 of the Fe-rich intermediate layer in the WSG can account for the macro-nutrient
440 consumption being double that in the AG, and for the amplitude of seasonal

biogeochemical variation in the WSG also being higher than that in the AG. The edges of both gyres have higher DFe/N ratios below the winter mixed layer water (e.g., at BD 4 in the west and P4, P12, and P16 in the east; Fig. 7c, Fig. 8); in these areas, high biological production leads to the observed surface nutrient decrease.

Although higher upward DFe supply occurs in the western part of North Pacific as described above, this biological production does not cause nutrient depletion in both subarctic gyres. To explain HNLC water formation, we compere the DFe and N+N upward supply stoichiometry to Fe and nitrate demand in surface waters. Marchetii et al. (2006) reported the minimum requirement of Fe/C mol ratio of dominant diatom *Pseudo-nitzschia* spp. in the subarctic Pacific is 2.8 to 3.7 μmol Fe/C mol. Sunda and Huntsman (1995) also reported the minimum ratio as ~3 μmol Fe/C mol for oceanic centric diatom *Thalassiosira oceanica*. Calculated from the Redfield ratio, the Fe/C ratio converts to a Fe/N ratio of 0.019-0.025 (nM/μM). These Fe/N demand ratios were compared to our obtained data from the section profiles in this study (Fig.9). Although a DFe to N+N plot (Fig. 9a) clearly shows that the increase of DFe concentration relative to N+N concentration from the surface to the intermediate water in the WSG (slope of dotted line in the Fig. 9a) is obviously higher than that of the CNP and the AG (slope of dotted line in the Fig. 9b-c), the absolute value of DFe to N+N concentration ratio in the Fe-rich intermediate water in the WSG does not reach the ratio of the Fe/N demand for the dominant diatom (solid line in the Fig. 9a-c), except at BD 4 (Fig. 9a). This relationship is also applicable if we take into consideration total dissolvable Fe fraction which include labile particulate Fe (Fig. 9 d-f). Although the existing form of the labile particulate Fe is not clear in this study, bioavailability of this fraction of Fe may be low, because surface consumption of N+N can be explained quantitatively by only DFe supply from below surface. Therefore, the

property of WSG water simultaneously explains the high amplitude of seasonal variation in biogeochemical parameters and the formation of HNLC water.

Fractionation between Fe and phosphate in shallow waters

In this studied area, Fe and other nutrients were mainly supplied via vertical mixing to the surface. Here, we compared vertical distributions of DFe with those of phosphate. The fractionation between trace metals and phosphate was discussed in surface water previously (Boyle et al. 1981). As a simple model, particulate materials (*PM*) remove the DFe (*Fe*) in water (*W*) via adsorption onto particles, aggregation of colloidal particles and biological uptake processes by a fractionation factor α relative to soluble reactive phosphorus (*P*):

$$\alpha = \frac{(Fe/P)_{PM}}{(Fe/P)_{W}}$$

Zooplankton and bacteria will take particulate material and recycle some of the particulate materials back into the water column. The remaining particulate material will be removed from the mixed layer as fast sinking material (*FM*). During this process, *Fe* and *P* will be fractionated as a function of β.

$$\beta = \frac{(Fe/P)_{FM}}{(Fe/P)_{PM}}$$

The fractionation factor between sinking material and the water transported to the euphotic zone can be represented with αβ. Depending on particles and environmental conditions, αβ will be variable. Assuming water deeper than the surface mixed layer is transported vertically with the initial concentrations Fe_0 and P_0, and both elements are removed without any addition, then

$$\frac{dFe}{dP} = \alpha\beta\left(\frac{Fe}{P}\right)$$

488 if αβ is constant, then

489 $$(\frac{Fe}{Fe_0}) = (\frac{P}{P_0})^{\alpha\beta}$$

490 We can arrange this equation to

491 $$\ln(\frac{Fe}{Fe_0}) = \alpha\beta \ln(\frac{P}{P_0})$$

492 Since the mixed layer is shallower than 200 m, here we assume that the concentration in
493 water at 200 m depth is the initial concentration. We plotted our DFe data relative to
494 phosphate in the subarctic Pacific (Fig. 10) and calculated the slopes (αβ). If αβ = 1, then
495 there is strict liner covariance between the *Fe* and *P* through the vertical processes (Fig.
496 10). If αβ < 1, the relation shows that *P* is removed more rapidly than *Fe*. If αβ > 1, then
497 the *Fe* removal is preferred over *P*.
498 We found linear relationship on these plots in the western, central and eastern
499 subarctic Pacific. In the WSG, the correlation became stronger when the data at 10 m
500 deep was removed (Fig. 10), which might implies that surface DFe concentrations in
501 the WSG are affected by atmospheric input of mineral dusts from the Asian continent.
502 As discussed above, we could not find a clear signature of atmospheric Fe in these
503 surface waters. Although our observed DFe in surface is low as < 0.1 nM, sporadic Fe
504 supply directly to the surface may also play a role in biological production in this
505 region; for example, it may account for sporadically occurring patchy phytoplankton
506 blooms, as reported by previous studies of waters characterized by high chlorophyll
507 concentrations, nutrients depletion, or both (Shiomoto et al. 1998; Bishop et al. 2002).
508 The comparison of *Fe* and *P* in the vertical profiles might show the slight signature of
509 atmospheric Fe, though the influences are very limited within the surface waters (in 10
510 m).

511 From the slopes in these plots, we estimated the fractionation factors between *Fe*
512 and *P*, αβ values, in the subarctic Pacific (Fig. 10). The αβ values are higher than 1 in
513 the subarctic Pacific, which indicates that DFe is preferentially removed from the
514 shallow waters compared with phosphate. To understand these αβ values, we applied
515 this analysis to DFe and PO_4 data from the Fe fertilization experiments in the subarctic
516 Pacific. Temporal variations of DFe and phosphate within the Fe-enriched patch were
517 applied to this analysis. In the subarctic Pacific, three Fe fertilization experiments were
518 performed, SEEDS-I and II in the western subarctic Pacific (Tsuda et al. 2003; 2007)
519 and SERIES in the eastern subarctic Pacific (Boyd et al. 2004). For this analysis
520 concerning the Fe fertilization experiments, we assumed the DFe and phosphate
521 concentrations at 5 m deep at the center of Fe-enriched patches at the initial day as Fe_0
522 and P_0, and analyzed their temporal variation of the fractionation between *Fe* and *P*.
523 For SEEDS-II and SERIES, we could not find clear relationship because Fe was
524 injected twice into the patches to stimulate the phytoplankton growth. On the other
525 hand, a single Fe injection was made during SEEDS-I. Here, we discuss only the results
526 from SEEDS-I where a linear relationship was obtained for *Fe* and *P* fractionation. The
527 αβ value was 3.94 $\pm$ 0.92, which is comparable to the vertical fractionation factor in
528 the WSG (Fig. 10). During the SEEDS-I experiment, the DFe concentration at 5 m deep
529 at the center of the Fe enriched patch was elevated to 2.9 nM, which is higher than DFe
530 concentrations in deep waters in this study. Even though the DFe concentration was
531 highly elevated, 0.66 μM of phosphate remained in water after 12 days. The
532 fractionation between *Fe* and *P* during the SEEDS-I experiments probably indicates
533 that DFe was preferentially removed compared with *P*.
534 The vertical fractionation of *Fe* and *P* in the WSG might be caused by the similar

process to SEEDS-I experiment (adsorption onto particles, aggregation of colloidal particles and biological uptake). In the CNP and AG, the fractionation factors were slightly smaller than that in the WSG (Fig. 10). The high fractionation factor in the WSG implies that vertically transported DFe is not effectively used for phytoplankton growth and/or preferentially scavenged from shallow waters. These processes may be related to incomplete consumption of nutrients even after entrainment in wintertime by deep vertical water mixing. This *Fe*/*P* fractionation analysis also indicates HNLC water formation in the subarctic Pacific. To understand the vertical fractionation of *Fe* and *P*, however, we also need more information on recycling of *Fe* and *P* within the euphotic zone. Moreover, chemical speciation and bioavailability of vertically transported Fe might be related to the fractionation. More detailed process studies will be needed to understand the biogeochemical cycles of Fe as a nutrient for phytoplankton growth in the ocean.

Conclusion

Judging from the west-to-east section profile of DFe in the western and central subarctic Pacific, the western subarctic Pacific received external DFe in the intermediate water and the Fe-rich intermediate water distributed across over 2000 km. The predominant source of Fe controlling the higher seasonal amplitude of variation in biogeochemical parameters in the western subarctic Pacific is Fe which is transported upward from the Fe-rich intermediate water to the surface layer via eddy diffusion and winter mixing. However, comparison of Fe to N+N stoichiometry between supply and demand, and analysis of *Fe*/*P* fractionation in shallow water, indicated that biological production stimulated by the upwelled Fe supply does not cause nutrient depletion in

559 the whole subarctic Pacific (in the WSG, the CNP, and the AG). Our findings from this
560 study clearly explain both HNLC water formation in the subarctic Pacific and high
561 amplitude of seasonal variation in biogeochemical parameters in the WSG,
562 simultaneously.
563
564
565 **Acknowledgements**
566 This work was carried out as part of the Japanese GEOTRACES program. We express our
567 thanks to Dr. T. Gamo for managing the program. We also thank all crew members and
568 participants in the R/V *Hakuho-maru* cruise. We thank Dr. S. Takano, Dr. T. Kim, Dr. N.
569 Nakayama, and Dr. S. Takeda, Ms A. Murayama for their assistance with the trace metal
570 sampling and the measurement of nutrients and dissolved oxygen. We thank Dr. K.
571 Bruland and Dr. G. Smith for providing the SAFe inter-calibration samples. This study was
572 supported by a Grant-in-Aid for Scientific Research (B) (No. 26281002) to JN, Grant-in-
573 Aid for Scientific Research in Innovative Areas (No.15H05820) from the Ministry of
574 Education, Culture, Sports, Science and Technology to JN and HO. This study was
575 supported partly by the Grant for Joint Research Program of the Institute of Low
576 Temperature Science, Hokkaido University.
577

References

Aguilar-Islas, A. M., M. P. Hurst, K. N. Buck, B. Sohst, G. J. Smith, M. C. Lohan, and K. W. Bruland. 2007. Micro- and macronutrients in the southeastern Bering Sea: Insight into iron-replete and iron-depleted regimes. Prog. Oceanogr. **73**: 99-126. doi:0.1016/j.pocean.2006.12.002

Bishop, J. K., R. E. Davis, and J. T. Sherman. 2002. Robotic observation of dust storm enhancement of carbon biomass in the North Pacific. Science **298**: 817-821.

Bograd, S. J., R. E. Thomson, A. B. Rabinovich, and P. H. LeBlond. 1999. Near-surface circulation of the northeast Pacific Ocean derived from WOCE-SVP satellite-tracked drifters. Deep Sea Res., Part II Top. Stud. Oceanogr. **46** (11-12): 2371-2403. doi:10.1016/S0976-0645(99)00068-5.

Boyd, P. W., S. Storm, F. A. Whitney, S. Doherty, M. E. Wen, P. J. Harrison, C. S. Wong, and D. E. Varela. 1995. The NE subarctic Pacific in winter: I Biological standing stocks. Mar. Ecol. Prog. Ser. **136**: 179-193.

Boyd, P. W., and P. J. Harrison. 1999. Phytoplankton dynamics in the NE subarctic Pacific. Deep Sea Res., Part II Top. Stud. Oceanogr. 46 (11-12): 2405-2432.

Boyd, P. W., C. S. Law, C. S. Wong, Y. Nojiri, A. Tsuda, M. Levasseur, S. Takeda, R. Rivkin, P. J. Harrison, R. Strzepek, J. Gower, R. M. McKay, E. Abraham, M. Arychuk, J. Barwell-Clarke, W. Crawford, M. Hale, K. Harada, K. Johnson, H. Kiyosawa, I. Kudo, A. Marchetti, W. Miller, J. Needoba, J. Nishioka, H. Ogawa, J. Page, M. Robert, H. Saito, A. Sastri, N. Sherry, T. Soutar, N. Sutherland, Y. Taira, F. Whitney, S. E. Wong, and T. Yoshimura. 2004. The decline and fate of an iron-induced subarctic phytoplankton bloom. Nature **428**: 549-553. doi:10.1038/nature02437

Boyd, P. W., and M. J. Ellwood. 2010. The biogeochemical cycle of iron in the ocean, Nat. Geosci. **3**: 675-682. doi:10.1038/ngeo964

Boyle, E. A., S. S. Huested, and S. P. Jones. 1981. On the distribution of cupper, nickel and cadmium in the surface water of the North Atlantic and North Pacific. J. Geophis. Res., C9, **86**: 8048-8066. doi:10.1029/JC086iC09p08048

Brown, M. T., W. M. Landing, C. I. Measures. 2005. Dissolved and particulate Fe in the western and central North Pacific: Results from the 2002 IOC cruise. Geochem., Geophys., Geosyst. **6**: Q10001. doi:10.1029/2004GC000893.

Bruland, K. W., K. J. Orians, and J. P. Cowen. 1994. Reactive trace metals in the stratified central North Pacific. Geochim. Cosmochim. Acta **58**(15): 3171-3182. doi:10.1016/0016-7037(94)90044-2

Buesseler, K. O., C. H. Lamborg, P. W. Boyd, P. J. Lam, T. W. Trull, R. R. Bidigare, J. K. B. Bishop, K. L. Casciotti, F. Dehairs, M. Elskens, M. Honda, D. M. Karl, D. A. Siegel, M. W. Silver, D. K. Steinberg, J. Valdes, B. Van Mooy, and S. Wilson. 2007. Revisiting carbon flux through the ocean's twilight zone. Science **316**:567-570. doi:10.1126/science.1137959. doi:10.1126/science.1137959

Chierici, M., A. Fransson, and Y. Nojiri. 2006. Biogeochemical processes as drivers of surface fCO_2 in contrasting provinces in the subarctic North Pacific Ocean. Global Biogeochem. Cycles **20**: GB1009, doi:10.1029/2004GB002356. doi:10.1029/2004GB002356

Conway T. M., and S. G. John. 2014. Quantification of dissolved iron sources to the North Atlantic Ocean. Nature **511**: 212‑215. doi:10.1038/nature13482.

Conway, T. M., and S. G. John. 2015. The cycling of iron, zinc and cadmium in the North East Pacific Ocean-Insights from stable isotopes. Geochem. Cosmochim. Acta. **164**: 262-283. doi:10.1016/j.gca.2015.05.023

Cullen, J. T., M. Chong, and D. Ianson. 2009. British Columbian continental shelf as a source of dissolved iron to the subarctic northeast Pacific Ocean. Global Biogeochem. Cycles. **23**: 1-12. doi:10.1029/2008GB003326.

Duce, R. A., and N. W. Tindale. 1991. Atmospheric transport of iron and its deposition in the ocean. Limnol. Oceanogr. **36**: 1715-1726. doi:10.4319/lo.1991.36.8.1715

Elrod, V. A., W. M. Berelson, K. H. Coale, and K. S. Johnson. 2004. The flux of iron from continental shelf sediment: A missing source for global budget. Geophys. Res. Lett. **31**: L12307. doi:10.1029/2004GL020216.

Elrod, V. A., K. S. Johnson, S. E. Fitzwater, and J. N. Plant. 2008. A long-term, high-resolution record of surface water iron concentrations in the upwelling-driven central California region. J. Geophys. Res. **113**: C11021. doi:10.1029/2007JC004610.

Emerson, S., Y. W. Watanabe, T. Ono, and S. Mecking. 2004. Temporal trends in apparent oxygen utilization in the upper pycnocline of the North Pacific: 1980-2000. J. Oceanogr. **60**: 139-147. doi:10.1023/B:JOCE.0000038323.62130.a0

Ezoe, M., T. Ishita, M. Kinugasa, X. Lai, K. Norisuye, and Y. Sohrin. 2004. Distribution of dissolved and acid-dissolvable bioactive trace metals in the North Pacific Ocean. Geochem. J. **38**: 535-550.

Fujiki, T., K. Matsumoto, Y. Mino, K. Sasaoka, M. Wakita, H. Kawakami, M. C. Honda, S. Watanabe, and T. Saino. 2014. Seasonal cycle of phytoplankton community structure and photophysiological state in the western subarctic gyre of the North Pacific. Limnol. Oceanogr. **59**(3): 887-900.

649 doi:10.4319/lo.2014.59.3.0887
650 Grand M. M., C. I. Measures, M. Hatta, W. T. Hiscock, C. S. Buck, and W. M.
651 Landing. 2015. Dust deposition in the eastern Indian Ocean: The ocean perspective
652 from Antarctica to the Bay of Bengal. Global Biogeochem. Cycles. **29**: 357-374.
653 doi:10.1002/2014GB004898.
654 Harrison, P. J., P. W. Boyd, D. E. Varela, S. Takeda, A. Shiomoto, and T. Odate.
655 1999. Comparison of factors controlling phytoplankton productivity in the NE and
656 NW subarctic Pacific. Prog. Oceanogr. **43**: 205-234. doi:10.1016/S0079-
657 6611(99)00015-4
658 Harrison, P. J., F. A. Whitney, A. Tsuda, H. Saito, and K. Tadokoro. 2004. Nutrient
659 and phytoplankton dynamics in the NE and NW gyres of the subarctic Pacific
660 Ocean. J. Oceanogr. **60**: 93-117. doi:10.1023/B:JOCE.0000038321.57391.2a
661 Hatta, M., C. I. Measures, S. Roshan, J. Wu, J. N. Fizsimmons, P. Sedwick, and P. L.
662 Morton. 2015. An overview of dissolved Fe and Mn distributions during the 2010-
663 2011 U. S. GEOTRACES North Atlantic cruises. Deep Sea Res. Part II Top. Stud.
664 Oceanogr. **116**: 117-129. doi:10.1016/j.dsr2.2014.07.005
665 Honda, M. C. 2003. Biological pump in northwestern North Pacific. J. Oceanogr. **59**:
666 671–684. doi:10.1023/B:JOCE.0000009596.57705.0c
667 Honda, M. C., K. Imai, Y. Nojiri, F. Hoshi, T. Sugawara, and M. Kusakabe. 2002.
668 The biological pump in the northwestern North Pacific based on fluxes and major
669 component of particulate matter obtained by sediment trap experiments (1997–
670 2000). Deep Sea Res. Part II Top. Stud. Oceanogr. **49**: 5595–5626.
671 doi:10.1016/S0967-0645(02)00201-1
672 Hurst, P.M., A.M. Aguilar-Islas, and K.W. Bruland. 2010. Iron in the southeastern
673 Bering Sea: elevated leachable particulate Fe in shelf bottom waters as an
674 important source for surface waters. Cont. Shelf Res. 30: 467‑480.
675 doi:10.1016/j.csr.2010.01.001
676 Imai, K., Y. Nojiri, N. Tsurushima, and T. Saino. 2002. Time series of seasonal
677 variation of primary productivity at station KNOT (44° N, 155° E) in the sub-arctic
678 western North Pacific. Deep Sea Res. Part II Top. Stud. Oceanogr. **49**: 5395-5408.
679 doi:10.1016/S0967-0645(02)00198-4
680 Isada, T., A. Hattori-Saito, H. Saito, T. Ikeda, and K. Suzuki. 2010. Primary
681 productivity and its bio-optical modeling in the Oyashio region, NW Pacific during
682 the spring bloom 2007. Deep Sea Res. Part II Top. Stud. Oceanogr. **57**: 1653-1664.
683 doi:10.1016/j.dsr2.2010.03.009
684 Jickells, T. D., Z. S. An, K. K. Andersen, A. R. Baker, G. Bergametti, N. Brooks, J. J.

685 Cao, P. W. Boyd, R. A. Duce, K. A. Hunter, H. Kawahata, N. Kubilay, J.
686 LaRoche, P. S. Liss, N. Mahowald, J. M. Prospero, A. J. Ridgwell, I. Tegen, and
687 R. Torres. 2005. Global iron connections between desert dust, ocean
688 biogeochemistry. Science **308**: 67-71. doi:10.1126/science.1105959
689 Johnson, K. S., Gordon, R. M. and Coale, K. H.: What controls dissolved iron in the
690 world ocean?, Mar. Chem., 57, 137–161, doi:10.1016/s0304-4203(97)00043-1,
691 1997. doi:10.1016/S0304-4203(97)00047-9
692 Johnson, K. S., F. P. Chavez, and G. E. Friedrich. 1999. Continental-shelf sediment as
693 a primary source of iron for coastal phytoplankton. Nature **398**: 697-700.
694 doi:10.1038/19511
695 Johnson, K. S., V. Elrod, S. Fitzwater, J. Plant, E. Boyle, B. Bergquist, K. Bruland, A.
696 Aguilar-Islas, K. Buck, M. Lohan, G. J. Smith, B. Sohst, K. Coale, M. Gordon, S.
697 Tanner, C. Measures, J. Moffet, K. Barbeau, A. King, A. Bowie, Z. Chase, J.
698 Callen, P. Laan, W. Landing, J. Mendez, A. Milne, H. Obata, T. Doi, L. Ossiander,
699 G. Sarthou, P. Sedwick, S. Van den Berg, L. Laglera- Baquer, J. Wu, and Y. Cai.
700 2007. Developing standards for dissolved iron in seawater. EOS **88** (11): 131-132.
701 doi:10.1029/2007EO110003
702 Kawakami, H., M. C. Honda, K. Matsumoto, M. Wakita, M. Kitamura, T. Fujiki, and
703 S. Watanabe. 2015. POC fluxes estimated from ^{234}Th in late spring-early summer
704 in the western subarctic North Pacific. J. Oceanogr. **71**:311–324.
705 doi:10.1007/s10872-015-0290-8
706 Kim, T., H. Obata, T. Gamo, J. Nishioka. 2015. Sampling and onboard analytical
707 methods for determining subnanomolar concentrations of zinc in seawater. Limnol.
708 Oceanogr.: Methods **13**: 30-39. doi:10.1002/lom3.10004
709 Kitayama, S., K. Kuma, E. Manabe, K. Sugie, H. Takata, Y. Isoda, K. Toya, S. Saito,
710 S. Takagi, Y. Kamei, and K. Sakaoka. 2009. Controls on iron distributions in the
711 deep water column of the North Pacific Ocean: Iron (III) hydroxide solubility and
712 marine humic-type dissolved organic matter. J. Geophys. Res. **114**: C08019.
713 doi:10.1029/2008JC004754.
714 Lam, P. J., and J. K. B. Bishop. 2008. The continental margin is a key source of iron
715 to the HNLC North Pacific Ocean. Geophys. Res. Lett. **35**: L07608.
716 doi:10.1029/2008GL033294.
717 Lam, P. J., J. K. B. Bishop, C. C. Henning, M. A. Marcus, G. A. Waychunas, and I.
718 Y. Fung. 2006. Wintertime phytoplankton bloom in the subarctic Pacific supported
719 by continental margin iron. Glob. Biogeochem. Cycles **20**: GB1006.
720 doi:10.1029/2005GB002557.

721 Lam, P. J., D. C. Ohnemus, and M. A. Marcus. 2012. The speciation of marine
722 particulate iron adjacent to active and passive continental margins. Geochim.
723 Cosmochim. Acta **80**: 108-124. doi:10.1016/j.gca.2011.11.044
724 Lippiatt, S. M., M. C. Lohan, K. W. Bruland. 2010. The distribution of reactive iron
725 in northern Gulf of Alaska coastal waters. Mar. Chem. **121**: 187-199.
726 doi:10.1016/j.marchem.2010.04.007
727 Lohan, M. C., and K. W. Bruland. 2008. Elevated Fe (II) and Dissolved Fe in hypoxic
728 shelf waters off Oregon and Washington: An enhanced source of iron to coastal
729 upwelling regimes. Environ. Sci. Technol. **42**: doi:10.1021/es800144j.
730 Marchetti, A., M. T. Maldonado, E. S. Lane, and P. J. Harrison. 2006. Iron
731 requirements of the pennate diatom Pseudo-nitzschia: Comparison of oceanic
732 (high-nitrate, low-chlorophyll waters) and coastal species. Limnol. Oceanogr.
733 **51**(5): 2092–2101.
734 Martin, J. H., and S. E. Fitzwater. 1988. Iron deficiency limits phytoplankton growth
735 in the north-east Pacific subarctic. Nature 331, 28, 341-343.
736 Martin, J. H., R. M. Gordon, S. Fitzwater, and W.W. Broenkow. 1989. VERTEX:
737 Phytoplankton/iron studies in the Gulf of Alaska. Deep Sea Res. Part I Oceanogr.
738 Res. Pap. **36**(5): 649–680. doi:10.1016/0198-0149(89)90144-1
739 Measures, C. I.. 1999. The role of entrained sediments in sea ice in the distribution of
740 aluminium and iron in the surface waters of the Arctic Ocean. Mar. Chem. **68**: 59-
741 70. doi:10.1016/S0304-4203(99)00065-1
742 Misumi, K., D. Tsumune, Y. Yoshida, K. Uchimoto, T. Nakamura, J. Nishioka, H.
743 Mitsudera, F. O. Brian, K. Lindsay, J. K. Moore, S. C. Doney. 2011.
744 Mechanisms controlling dissolved iron distribution in the North Pacific: a model
745 study. J. Geophys. Res. **116**, G03005. doi:10.1029/2010JG001541.
746 Mochizuki, M., N. Shiga, M. Saito, K. Imai, and Y. Nojiri. 2002. Seasonal changes in
747 nutrients, chlorophyll a and the phytoplankton assemblage of the western subarctic
748 gyre in the Pacific Ocean. Deep Sea Research Part II Top. Stud. Oceanogr. **49**:
749 5241-5439. doi:10.1016/S0967-0645(02)00209-6
750 Nakanowatari, T., K. I. Ohshima, M. Wakatsuchi. 2007. Warming and oxygen
751 decrease of intermediate water in the northwestern North Pacific, originating from
752 the Sea of Okhotsk, 1955-2004. Geophys. Res. Lett. 34, L04602.
753 doi:10.1029/2006GL028243.
754 Nishioka, J., S. Takeda, C. S. Wong, and W. K. Johnson. 2001. Size-fractionated iron
755 concentrations in the northeast Pacific Ocean: distribution of soluble and small
756 colloidal iron. Mar. Chem. **74**: 157-179. doi:10.1016/S0304-4203(01)00013-5

Nishioka, J., S. Takeda, I. Kudo, D. Tsumune, T. Yoshimura, K. Kuma, and A. Tsuda. 2003. Size-fractionated iron distributions and iron-limitation processes in the subarctic NW Pacific. Geophys. Res. Lett. **30**(14), 1730. doi:10.1029/2002GL016853.

Nishioka, J., T. Ono, H. Saito, T. Nakatsuka, S. Takeda, T. Yoshimura, K. Suzuki, K. Kuma, S. Nakabayashi, D. Tsumune, H. Mitsudera, Wm. K. Johnson, and A. Tsuda. 2007. Iron supply to the western subarctic Pacific: Importance of iron export from the Sea of Okhotsk. J. Geophys. Res. Oceans **112**: C10012 doi:10.1029/2006JC004055.

Nishioka, J., T. Ono, H. Saito, K. Sakaoka, and T. Yoshimura. 2011. Oceanic iron supply mechanisms which support the spring diatom bloom in the Oyashio region, western subarctic Pacific. J. Geophys. Res. Oceans **116**. C02021 doi: 10.1029/2010JC006321.

Nishioka, J., T. Nakatsuka, Y. W. Watanabe, I. Yasuda, K. Kuma, H. Ogawa, N. Ebuchi, A. Scherbinin, Y. N. Volkov, T. Shiraiwa, and M. Wakatsuchi. 2013a. Intensive mixing along an island chain controls oceanic biogeochemical cycles. Glob. Biogeochem. Cycle **27**:920-929. doi:10.1002/gbc.20088.

Nishioka, J., H. Obata, and D. Tsumune. 2013b. Evidence of an extensive spread of hydrothermal dissolved iron in the Indian Ocean. Earth Planet. Sci. Lett. **361**: 26-33. doi:10.1016/j.epsl.2012.11.040.

Obata, H., H. Karatani, and E. Nakayama. 1993. Automated determination of iron in seawater by chelating resin concentration and chemiluminescence detection. Anal. Chem. **65**: 1524 – 1528.

Obata, H., H. Karatani, M. Matsui and E. Nakayama, 1997. Fundamental studies for chemical speciation of iron in seawater with an improved analytical method. Mar. Chem. **56**: 97-106. doi:10.1016/S0304-4203(96)00082-5

Parekh, P., M. J. Follows, and E. A. Boyle. 2005. Decoupling of iron and phosphate in the global ocean. Glob. Biogeochem. Cycle **19**: GB2020. doi:10.1029/2004GB002280.

Reid, J. L. 1965. Intermediate water of the Pacific Ocean. Johns Hopkins Oceanogr. Stud., 2, 85 pp.

Resing, J. A. P. N. Sedwick, C. R. German, W. J. Jenkins, J. W. Moffett, B. M. Sohst, and A. Tagliabue. 2015. Basin-scale transport of hydrothermal dissolved metals across the South Pacific Ocean. Nature **523**: 200-203. doi:10.1038/nature14577.

Rijkenberg, M. A., R. Middag, P. Laan, L. J. A. Gerringa, H. M. van Aken, V. Schoemann, J. T. M. de Jong, and H. J. W. Baar. 2014. The distribution of

793 dissolved iron in the west Atlantic Ocean. PLoS One **9**:
794 doi:10.1371/journal.pone.0101323.
795 Sarmiento, J. L. and N. Gruber, Ocean biogeochemical dynamics, Prinston University
796 press, pp 503 .
797 Shiomoto, A., and H. Asami. 1999. High-West and Low-East distribution patterns of
798 chlorophyll a. primary productivity and diatoms in the subarctic North Pacific
799 surface waters, mid winter 1996. J. Oceanogr. **55**: 493-503.
800 doi:10.1023/A:1007835306413
801 Shiomoto, A., Y. Ishida, M. Tamaki, and Y. Yamanaka. 1998. Primary production
802 and chlorophyll a in the NW pacific ocean in summer. J. Geophys. Res. Ocean
803 **103**: 24651-24661. doi:10.1029/98JC01538
804 Smith, K. l., B. H. Robinson, J. J. Helly, R. S. Kaufmann, H. A. Ruhl, T. J. Shaw, B.
805 S. Twining, and M. Vernet. 2007. Free-drifting icebergs: Hot spots of chemical
806 and biological enrichment in the Weddell Sea. Science **317**: 478-482.
807 doi:10.1126/science.1142834
808 Suga, T., K. Motoki, and Y. Aoki. 2004. The North Pacific climatology of winter
809 mixed layer and mode waters. J. Phys. Oceanogr. **34**: 3-22. doi:10.1175/1520-
810 0485(2004)034<0003:TNPCOW>2.0.CO;2
811 Sunda, W. G., and S. A. Huntsman. 1995. Iron uptake and growth limitation in
812 oceanic and coastal phytoplankton. Mar. Chem. **50**: 189-206. doi:10.1016/0304-
813 4203(95)00035-P
814 Suzuki, K., H. Liu, T. Saino, H. Obata, M. Takano, K. Okamura, Y. Sohrin, and Y.
815 Fujishima. 2002. East-west gradients in the photosynthetic potential of
816 phytoplankton and iron concentration in the subarctic Pacific Ocean during early
817 summer. Limnol. Oceanogr. **47**(6): 1581-1594. doi:10.4319/lo.2002.47.6.1581
818 Tagliabue, A., J-B, Sallée, A. R. Bowie, M. Lévy, S. Swart, and P. W. Boyd. 2014a.
819 Surface-water iron supplies in the Southern Ocean sustained by deep winter mixing.
820 Nat. Geosci. **7**: 314-320. doi:10.1038/ngeo2101
821 Tagliabue, A., O. Aumont, and L. Bopp. 2014b. The impact of different external
822 sources of iron on the global carbon cycle. Geophys. Res. Lett. **41**: 920–926.
823 doi:10.1002/2013GL059059.
824 Takahashi, T., S. C. Sutherland, C. Sweeney, A. Poisson, N. Metzl, B. Tilbrook, N.
825 Bates, R. Wanninkhof, R. A. Feely, C. Sabine, J. Olafsson, and Y. Nojiri. 2002.
826 Global sea-air CO_2 flux based on climatological surface ocean pCO_2, and seasonal
827 biological and temperature effects. Deep Sea Res. Part II Top. Stud. Oceanogr. **49**:
828 1601-1622. doi:10.1016/S0967-0645(02)00003-6

Takata, H., K. Kuma, S. Iwade, Y. Yamajoh, A. Yamaguchi, S. Takagi, K. Sakaoka, Y. Yamashita, E. Tanoue, T. Midorikawa, K. Kimura, and J. Nishioka. 2004. Spatial variability of iron in the surface water of the northwestern North Pacific Ocean. Mar. Chem. **86**: 139-157. doi:10.1016/j.marchem.2003.12.007

Takata, H., K. Kuma, Y. Saito, M. Cikira, S. Saito, Y. Isoda, S. Takagi, and K. Sakaoka. 2006. Comparing the vertical distribution of iron in the eastern and western North Pacific Ocean. Geophys. Res. Lett. **33**: doi:10.1029/2005GL024538.

Talley, L. D. 1991. An Okhotsk sea water anomaly: Implication for ventilation in the North Pacific. Deep Sea Res. Part I Oceanogr. Res. Pap. **38**: S171-190. doi:10.1016/S0198-0149(12)80009-4

Talley, L. D. 2008. Freshwater transport estimate and the global overturning circulation: Shallow, deep and throughflow components. Prog. Oceanogr. **78**: 257-303. doi:10.1016/j.pocean.2008.05.001

Tsuda, A., S. Takeda, H. Saito, J. Nishioka, Y. Nojiri, I. Kudo, H. Kiyosawa, A. Shiomoto, I. Imai, T. Ono, A. Shimamoto, D. Tsumune, T. Yoshimura, T. Aono, A. Hinuma, M. Kinugasa, K. Suzuki, Y. Sohrin, Y. Noiri, H. Tani, D. Deguchi, N. Tsurushima, H. Ogawa, K. Fukami, K. Kuma, and T. Saino. 2003. A mesoscale iron enrichment in the western subarctic Pacific induces large centric diatom bloom. Science **300**: 958-961. doi:10.1126/science.1082000

Tsuda, A., S. Takeda, H. Saito, J. Nishioka, I. Kudo, Y. Nojiri, K. Suzuki, M. Uematsu, M.L. Wells., D. Tsumune, T. Yoshimura, T. Aono, T. Aramaki, W.P. Cochlan, M. Hayakawa, K. Imai, T. Isada, Y. Iwamoto, W.K. Johnson, S. Kameyama, S. Kato, H. Kiyosawa, Y. Kondo, M. Levasseur, R. Machida, I. Nagao, F. Nakagawa, T. Nakanishi, S. Nakatsuka, A. Narita, Y. Noiri, H. Obata, H. Ogawa, K. Oguma, T. Ono, T. Sakuragi, M. Sasakawa, M. Sato, A. Shimamoto, H. Takada, C.G. Trick, Y.W. Watanabe, C.S. Wong, and N. Yoshie. 2007. Evidence for the grazing hypothesis: Grazing reduces phytoplankton responses of the HNLC ecosystem to iron enrichment in the western subarctic Pacific (SEEDS II). J. Oceanogr., **63**: 983-994. doi:10.1007/s10872-007-0082-x

Tsurushima, N., Y. Nojiri, K. Imai, and S. Watanabe. 2002. Seasonal variations of carbon dioxide system and nutrients in the surface mixed layer at station KNOT (44ºN, 155ºE) in the subarctic western North Pacific. Deep-Sea Res. Part II Top. Stud. Oceanogr. **49**: 5377-5394.

Uchida, R., K. Kuma, A. Omata, S. Ishikawa, N. Hioki, H. Ueno, Y. Isoda, K. Sakaoka, Y. Kamei, and S. Takagi. 2013. Water column iron dynamics in the subarctic North Pacific Ocean and the Bering Sea. J. Geophys. Res. Oceans **118**:

1257-1271. doi:10.1002/jgrc.20097.
Uehara, H., A. A. Kruts, H. Mitsudera, T. nakamura, Y. N. Volkov and M. Wakatsuchi. 2014. Remotely propagating salinity anomaly varies the source of North Pacific ventilation. Prog. Oceanogr. 126, 80-97, doi:10.1016/j.pocean.2014.04.016.
Uematsu, M., R. A. Duce, J. M. Prospero, L. Q. Chen, J. T. Merrill, and R. L. McDonald. 1983. Transport of mineral aerosol from Asia over the North Pacific Ocean. J. Geophys. Res. **88** C9: 5343-5352.
Uematsu, M., A. Yoshikawa, H. Muraki, K. Arao, and I. Uno. 2002. Transport of mineral and anthropogenic aerosols during a Kosa event over East Asia. J. Oceanogr. **107**: D7. 4059. doi:10.1029/2001JD000333.
Watanabe, Y. W., M. Shigemitsu, and K. Tadokoro. 2008. Evidence of a change in oceanic fixed nitrogen with decadal climate change in the North Pacific subpolar region. Geophys. Res. Lett. **35**. doi:10.1029/2007GL032188.
Whitney, F. A. 2011. Nutrient variability in the mixed layer of the subarctic Pacific Ocean. 1987-2010. J. Oceanogr. **67**: doi10.1007/s10872-011-0051-2.
Whitney, F. A., and H. J. Freeland. 1999. Variability in upper-ocean water properties in the NE Pacific Ocean. Deep Sea Res. Part II Top. Stud. Oceanogr. **46**: 2351-2370. doi:10.1016/S0967-0645(99)00067-3
Wong, C. S., F. A. Whitney, D. W. Crawford, K. Iseki, R. J. Matear, W. K. Johnson, J. S. Page, and D. Timothy. 1999. Seasonal and interannual variability in particle fluxes of carbon, nitrogen and silicon from time series of sediment traps at Ocean station P, 1982-1993: relationship to changes in subarctic primary productivity. Deep Sea Res. I Oceanogr. Res. Pap. **46**: 2735-2760. doi:10.1016/S0967-0645(99)00082-X
Wu, J., A. Aguilar-Islas, R. Rember, T. Weingartner, S. Danielson and T. Whitledge. 2009. Size-fractionated iron distribution on the northern Gulf of Alaska. Geophys. Res. Lett. **36**: doi:10.1029/2009GL038304.
Yasuda, I. 1997. The origin of the North Pacific intermediate water. J. Geophysi. Res. Oceans **102**: 893-909. doi:10.1029/96JC02938
Yasuda, I. 2004. North Pacific intermediate water: Progress in SAGE (SubArctic Gyre Experiment) and related project. J. Oceanogr. 60, 385-395. doi:110.1023/B:JOCE.0000038344.25081.42
Yasunaka, S., Y. Nojiri, S. Nakaoka, T. Ono, F. A. Whitney, and M. Telszewski. 2014. J. Geophysi. Res. Oceans **119**: 7756-7771, doi:10.1002/2014JC010318.

Figure captions

Figure 1

Map showing sampling site in the subarctic Pacific. Circles and squares indicate vertical section sampling site observed in Japanese-GEOTRACES study in the subarctic Pacific, and data from circles are reported in this study. Black triangles indicate locations with previously reported data for dissolved Fe and nutrients along line P in the Alaskan gyre (P04, P12, P16, P20: Nishioka et al, 2001; Ocean station Papa (OSP) = T7: Martin et al., 1989). We define observed water to Oyashio-Kuroshio Transition Zone (OKTZ; BD 4, BD 5; in yellow circles), Western Subarctic Gyre (WSG; BD 6, BD 7, BD 8, BD 9; in red circles), Central subarctic North Pacific (CNP; BD 11, BD 13, BD 14; in green circles), and Alaskan Gyre (AG; BD 15, BD 16, T7, P 20; in black circles and triangles), and Alaskan Stream (AS; P16, P12, P04 in black triangles). Historical time series station KNOT, K2 in the WSG and station P in the AG are same location as BD 6, BD 7 and T7 in this study.

Figure 2

Vertical section profiles including all stations from BD 4 to BD16, except BD 10 and BD 12, (in Fig. 1) in the subarctic Pacific, (a) temperature, (b) salinity, (c) dissolved oxygen. White line in the (c) panel indicates isopycnal surface of 26.6 σ_θ and 27.5 σ_θ. We define observed water to Oyashio-Kuroshio Transition Zone (OKTZ; BD 4, BD 5), Western Subarctic Gyre (WSG; BD 6, BD 7, BD 8, BD 9), Central subarctic North Pacific (CNP; BD 11, BD 13, BD 14), and Alaskan Gyre (AG; BD 15, BD 16). This figure is drawn using ODV (https://odv.awi.de/en/home/).

Figure 3

Surface nitrate+nitrite and silicate (a) and dissolved Fe (b) average concentrations at 10 m and 25 m in the surface waters along the transect in this study. <DL mean data below detection limit. Error bar indicate SD for 10 m and 25 m value.

Figure 4

Vertical section profiles including all stations from BD 4 to BD 16, except BD 10 and BD 12, (in Fig. 1) in the subarctic Pacific, (a) nitrate+nitrite (μM), (b) phospate (μM), (c) silicate (μM). In each panel (a), (b) and (c), upper panel show 0 m to 500 m and lower panel show 0 m to bottom. This figure is drawn using ODV (https://odv.awi.de/en/home/).

Figure 5

Vertical profiles of dissolved Fe concentrations (a) at stations BD 4, BD 5 in the Oyashio-Kuroshio Transition Zone (OKTZ), (b) at stations BD 6, BD 7, BD 8, BD 9 in the Western Subarctic Gyre (WSG), (c) at stations BD10, BD12, (d) at stations BD11, BD13, BD14 in the Central subarctic North Pacific (CNP), (e) at stations BD15, BD16 in the Alaskan Gyre (AG). Vertical profiles of total dissolvable Fe concentrations (f) at BD 7, BD 9, (g) at BD11, BD14, BD15. In these vertical profiles, bottom sample depth was always generally 10 m off from the bottom.

Figure 6

Vertical section profiles including all stations from BD 4 to BD16, except BD 10 and BD 12, (in Fig. 1) in the subarctic Pacific, (a) dissolved Fe (nM), (b) Fe* index. In panel (a), upper panel shows 0 m to 500 m and lower panel shows 0 m to bottom. This figure is drawn using ODV (https://odv.awi.de/en/home/).

Figure 7

Dissolved Fe concentration/depth gradient (a), (*d*Fe/*dz*), nitrate+nitrite concentration/depth gradient (b), (*d*N/*dz*), and ratio of the dissolved Fe and nitrate+nitrite gradient (c), (*d*Fe/*dz*)/ (*d*N/*dz*), below surface mixed layer at stations BD 4, BD 5, BD 6, BD 7, BD 8, BD 9, BD11, BD13, BD14, BD15, BD16, and line P (OKTZ: Oyasio-Kuroshio Transition Zone, WSG: Western Subarctic Gyre, CNP: Central subarctic North Pacific, AG: Alaskan Gyre, AS: Alaskan Stream)

Figure 8

Vertical section profile of dissolved Fe and nitrate+nitrite concentration ratio including all stations from BD 4 to BD16, except BD 10 and BD 12, and line P (in Fig. 1) in the subarctic Pacific. The solid white lines in the figure indicate the 26 and 26.6 σ_θ isopycnal surfaces which are indicating bottom of winter mixed layer in the Alaskan Gyre (AG) and Oyasio-Kuroshio Transition Zone (OKTZ) + Western Subarctic Gyre (WSG), respectively. Upper panel shows 0 m to 400 m and lower panel show 0 m to bottom. Line P data is cited from Martin et al. 1989 and Nishioka et al. 2001. This figure is drawn using ODV (https://odv.awi.de/en/home/).

Figure 9

Comparison of sub-surface Fe to nitrate+nitrite (N+N) ratio with Fe and nutrient demand in surface diatom. Plots of dissolved Fe (DFe) versus N+N, (a) for data from the Oyashio-Kuroshio Transition Zone (OKTZ) and the Western Subarctic Gyre (OKTZ+WSG:BD 4, BD 5, BD 6, BD 7, BD 8, BD 9), (b) for data from Central North Pacific (CNP: BD 11, BD 13, BD 14) and (c) for data from Alaskan Gyre (AG: BD 15, BD 16, T7 (Martin et al. 1989), P20 (Nishioka et al., 2001). Plots of total dissolvable Fe (TDFe) versus nitrate+nitrite (N+N), (d) for data from WSG (BD 7, BD 9), (e) for CNP (BD 11, BD 14), and (f) for AG (BD 15). Solid line indicates Fe(nM)/N(μM) = 0.019, which is calculated by using reported minimum Fe demand (Marchetii et al. 2006). Dotted line indicates Fe(nM)/N(μM) increasing ratio in the water column from surface to intermediate waters.

Figure 10

Evaluation of Fe and PO_4 fractionation in the upper 200 m. Plots of ln (P/P_0) vs ln(Fe/Fe_0) (a) in the Western Subarctic Gyre (WSG), (b) in the Central North Pacific (CNP), and (c) in the Alaskan Gyre (AG) in shallower than 200 m. P_0 and Fe_0 are initial concentrations in waters at 200 m deep. Plot in brackets (or indicated by dashed line) indicates the data at 10 m in each profile.

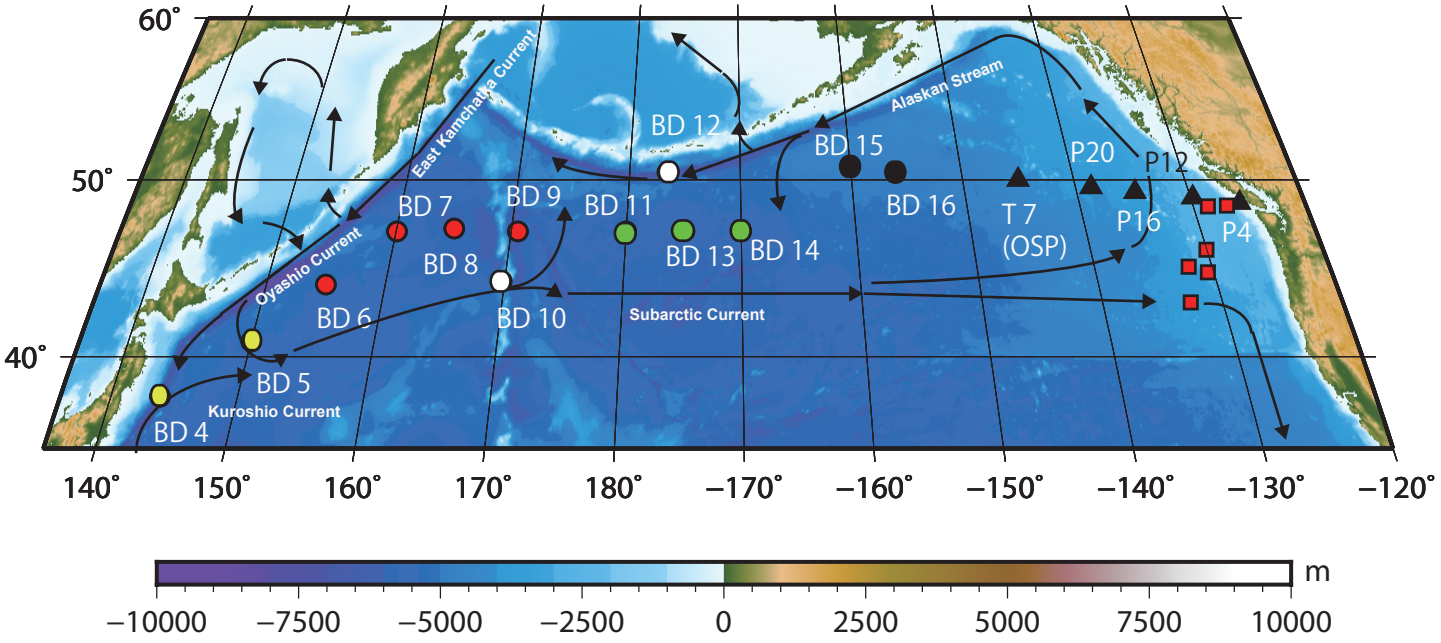


Figure 1

Map showing sampling site in the subarctic Pacific. Circles and squares indicate vertical section sampling site observed in Japanese-GEOTRACES study in the subarctic Pacific, and data from circles are reported in this study. Black triangles indicate locations with previously reported data for dissolved Fe and nutrients along line P in the Alaskan gyre (P04, P12, P16, P20: Nishioka et al, 2001; Ocean station Papa (OSP) = T7: Martin et al., 1989). We define observed water to Oyashio-Kuroshio Transition Zone (OKTZ; BD 4, BD 5; in yellow circles), Western Subarctic Gyre (WSG; BD 6, BD 7, BD 8, BD 9; in red circles), Central subarctic North Pacific (CNP; BD 11, BD 13, BD 14; in green circles), and Alaskan Gyre (AG; BD 15, BD 16, T7, P 20; in black circles and triangles), and Alaskan Stream (AS; P16, P12, P04 in black triangles). Historical time series station KNOT, K2 in the WSG and station P in the AG are same location as BD 6, BD 7 and T7 in this study.

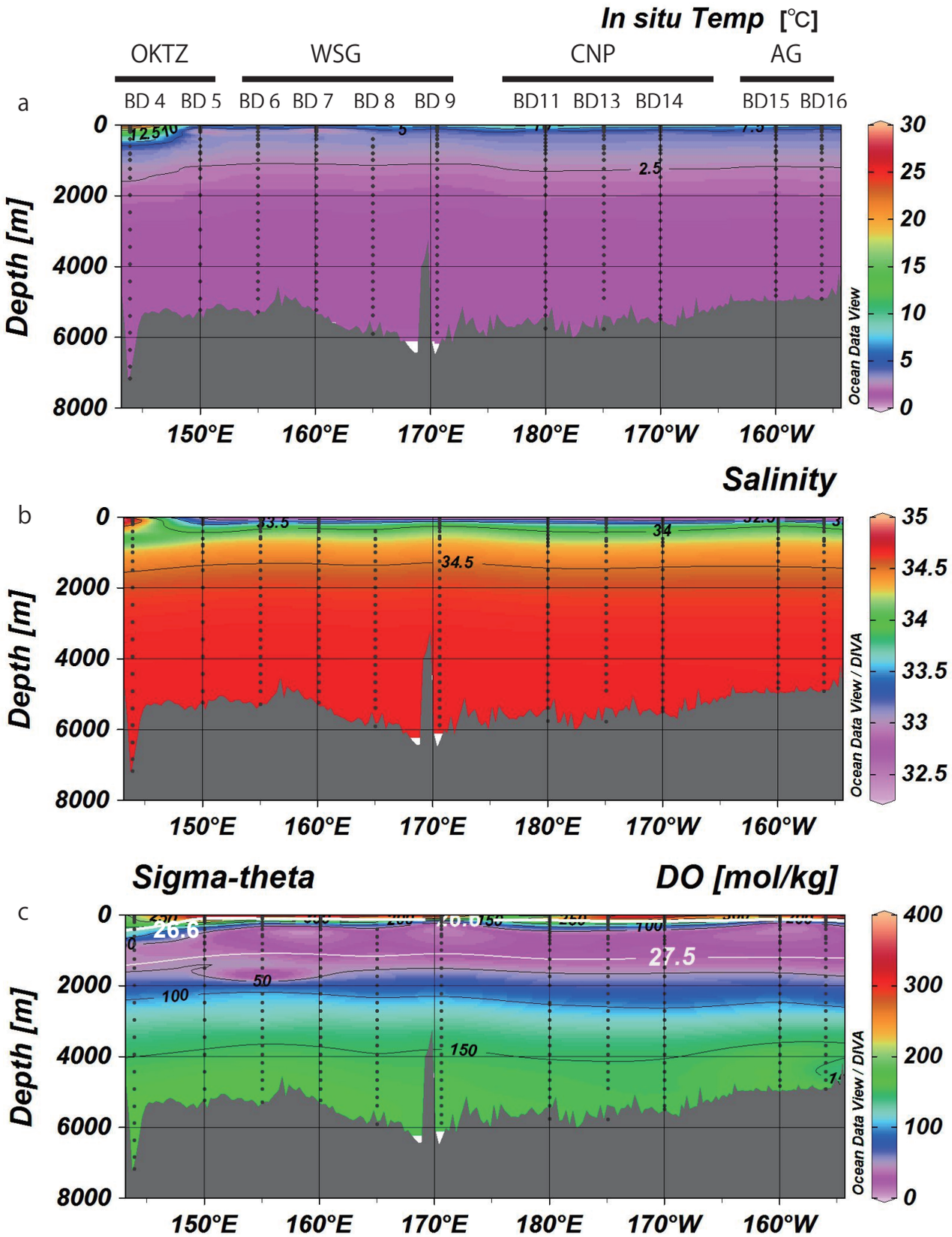


Figure 2

Vertical section profiles including all stations from BD 4 to BD16, except BD 10 and BD 12, (in Fig. 1) in the subarctic Pacific, (a) temperature, (b) salinity, (c) dissolved oxygen. White line in the (c) panel indicates isopycnal surface of 26.6 σ_θ and 27.5 σ_θ. We define observed water to Oyashio-Kuroshio Transition Zone (OKTZ; BD 4, BD 5), Western Subarctic Gyre (WSG; BD 6, BD 7, BD 8, BD 9), Central subarctic North Pacific (CNP; BD 11, BD 13, BD 14), and Alaskan Gyre (AG; BD 15, BD 16). This figure is drawn using ODV (https://odv.awi.de/en/home/).

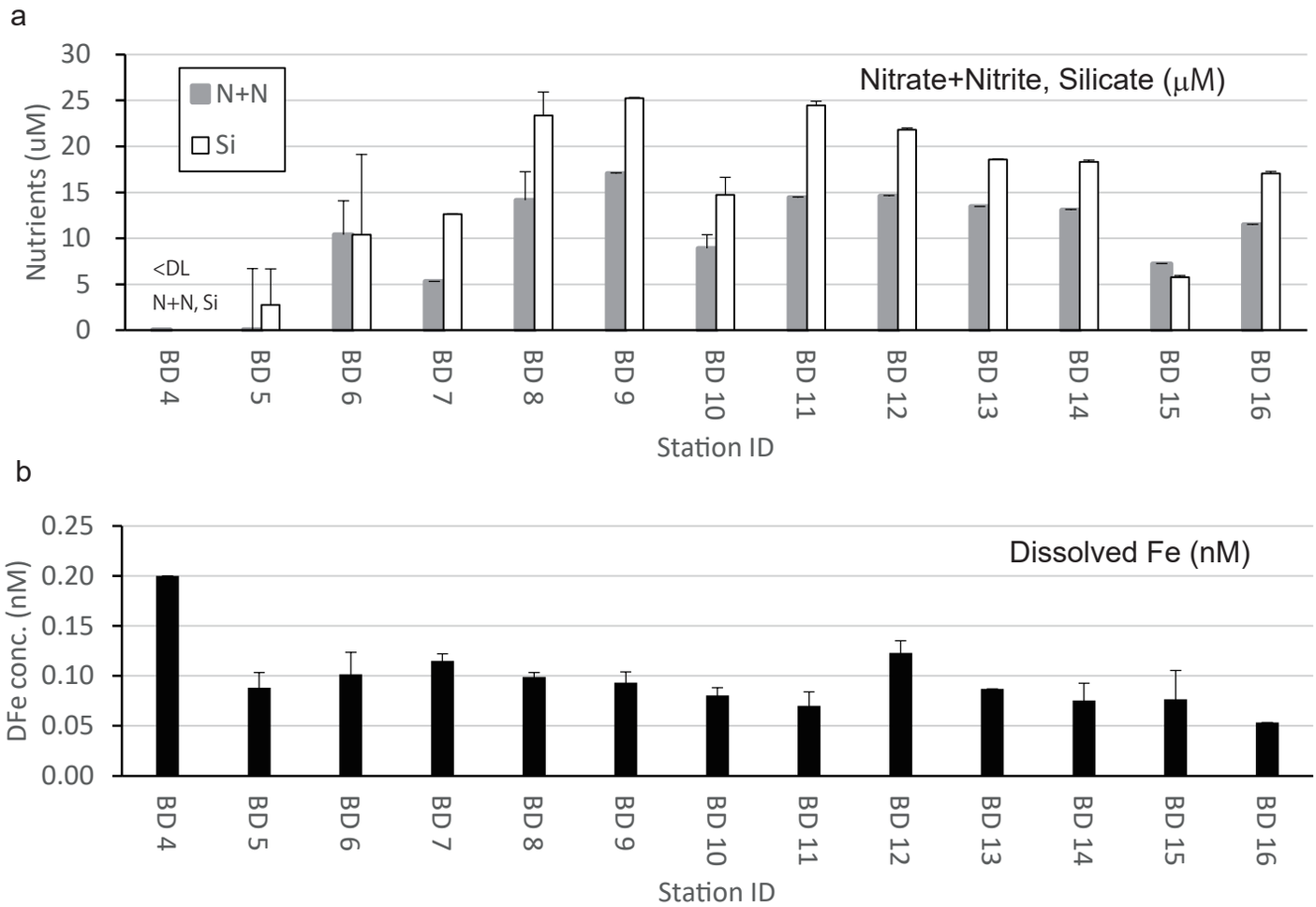


Figure 3

Surface nitrate+nitrite and silicate (a) and dissolved Fe (b) average concentrations at 10 m and 25 m in the surface waters along the transect in this study. <DL mean data below detection limit. Error bar indicate SD for 10 m and 25 m value.

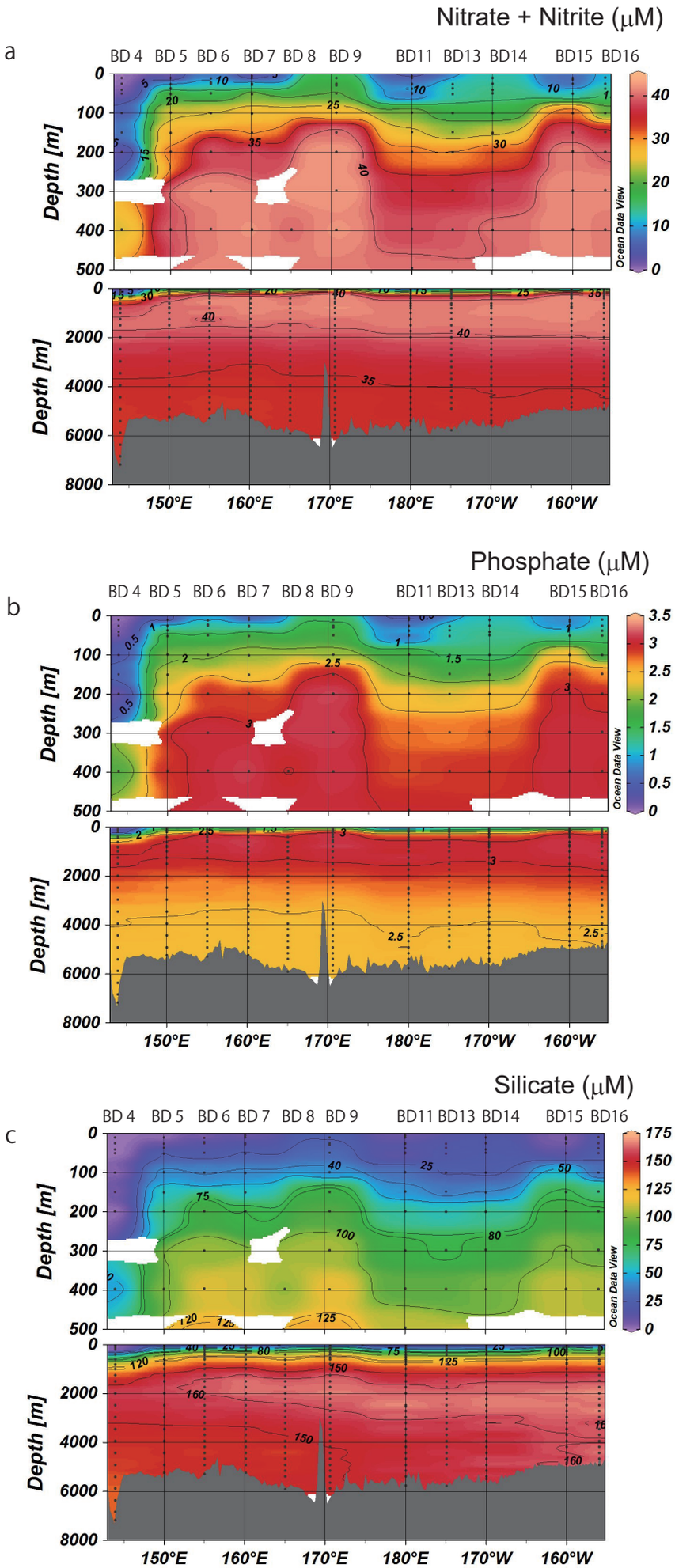


Figure 4

Vertical section profiles including all stations from BD 4 to BD 16, except BD 10 and BD 12, (in Fig. 1) in the subarctic Pacific, (a) nitrate+nitrite (μM), (b) phospate (μM), (c) silicate (μM). In each panel (a), (b) and (c), upper panel show 0 m to 500 m and lower panel show 0 m to bottom. This figure is drawn using ODV (https://odv.awi.de/en/home/).

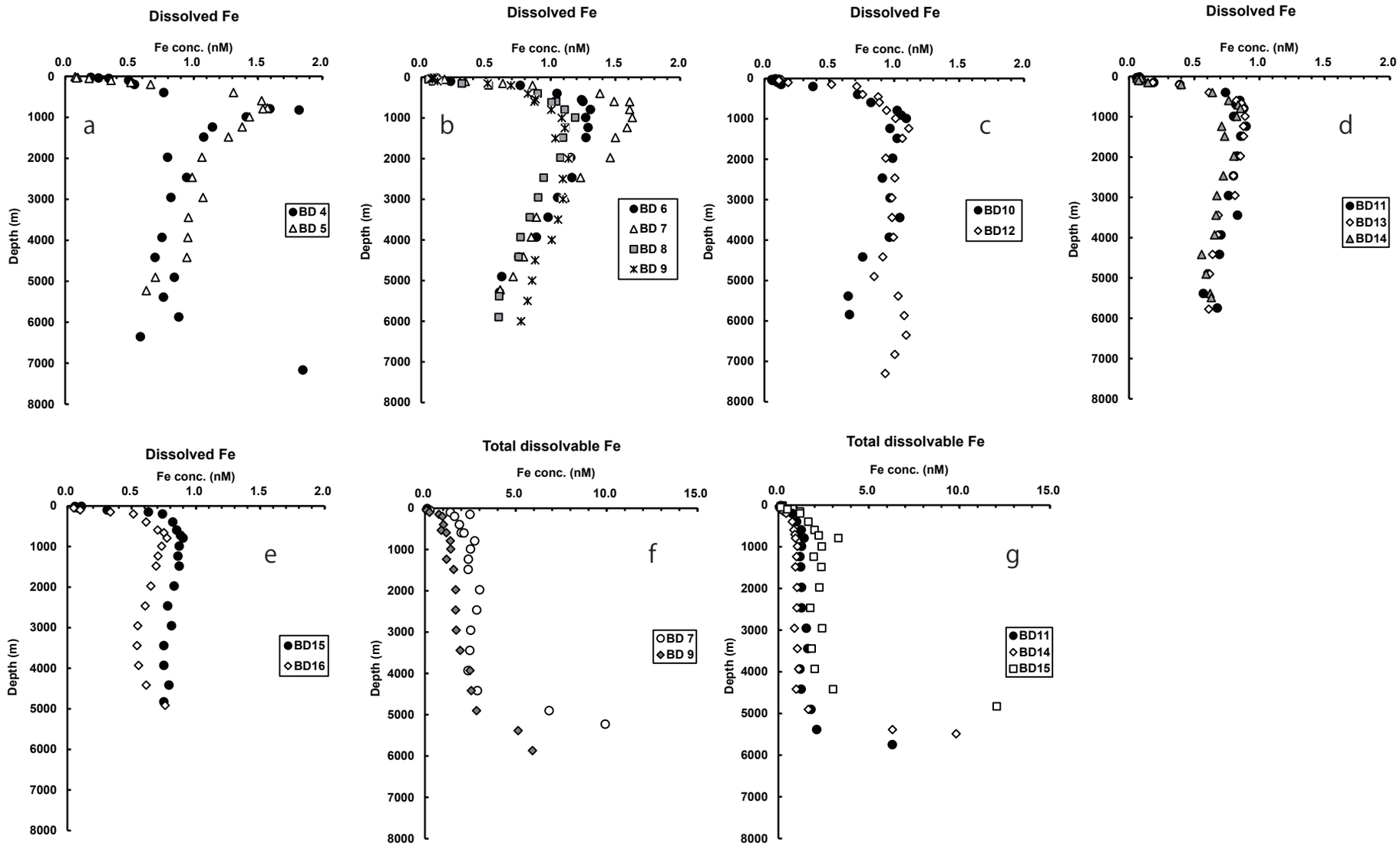


Figure 5

Vertical profiles of dissolved Fe concentrations (a) at stations BD 4, BD 5 in the Oyashio-Kuroshio Transition Zone (OKTZ), (b) at stations BD 6, BD 7, BD 8, BD 9 in the Western Subarctic Gyre (WSG), (c) at stations BD10, BD12, (d) at stations BD11, BD13, BD14 in the Central subarctic North Pacific (CNP), (e) at stations BD15, BD16 in the Alaskan Gyre (AG). Vertical profiles of total dissolvable Fe concentrations (f) at BD 7, BD 9, (g) at BD11, BD14, BD15. In these vertical profiles, bottom sample depth was always generally 10 m off from the bottom.

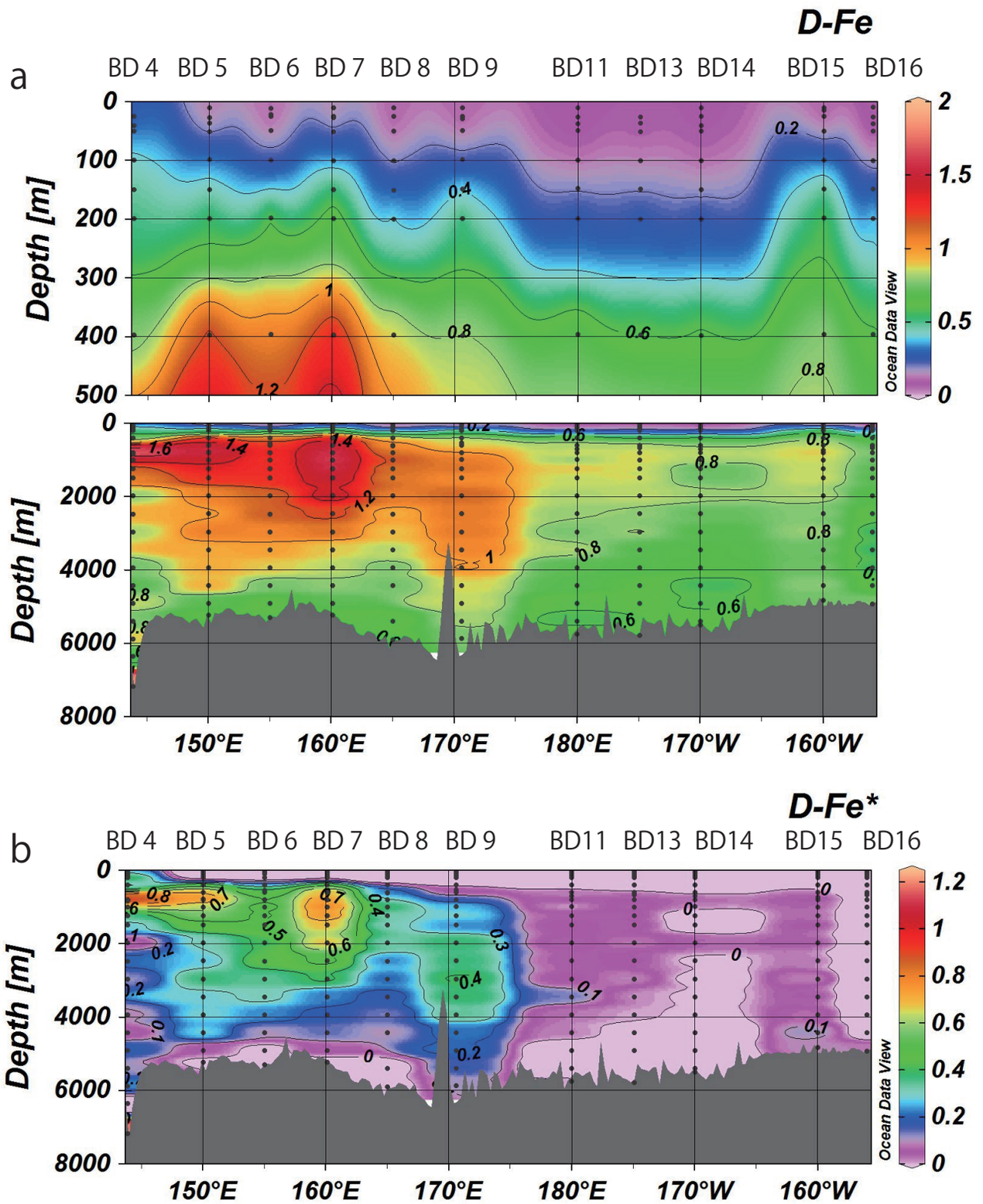


Figure 6

Vertical section profiles including all stations from BD 4 to BD16, except BD 10 and BD 12, (in Fig. 1) in the subarctic Pacific, (a) dissolved Fe (nM), (b) Fe* index. In panel (a), upper panel shows 0 m to 500 m and lower panel shows 0 m to bottom. This figure is drawn using ODV (https://odv.awi.de/en/home/).

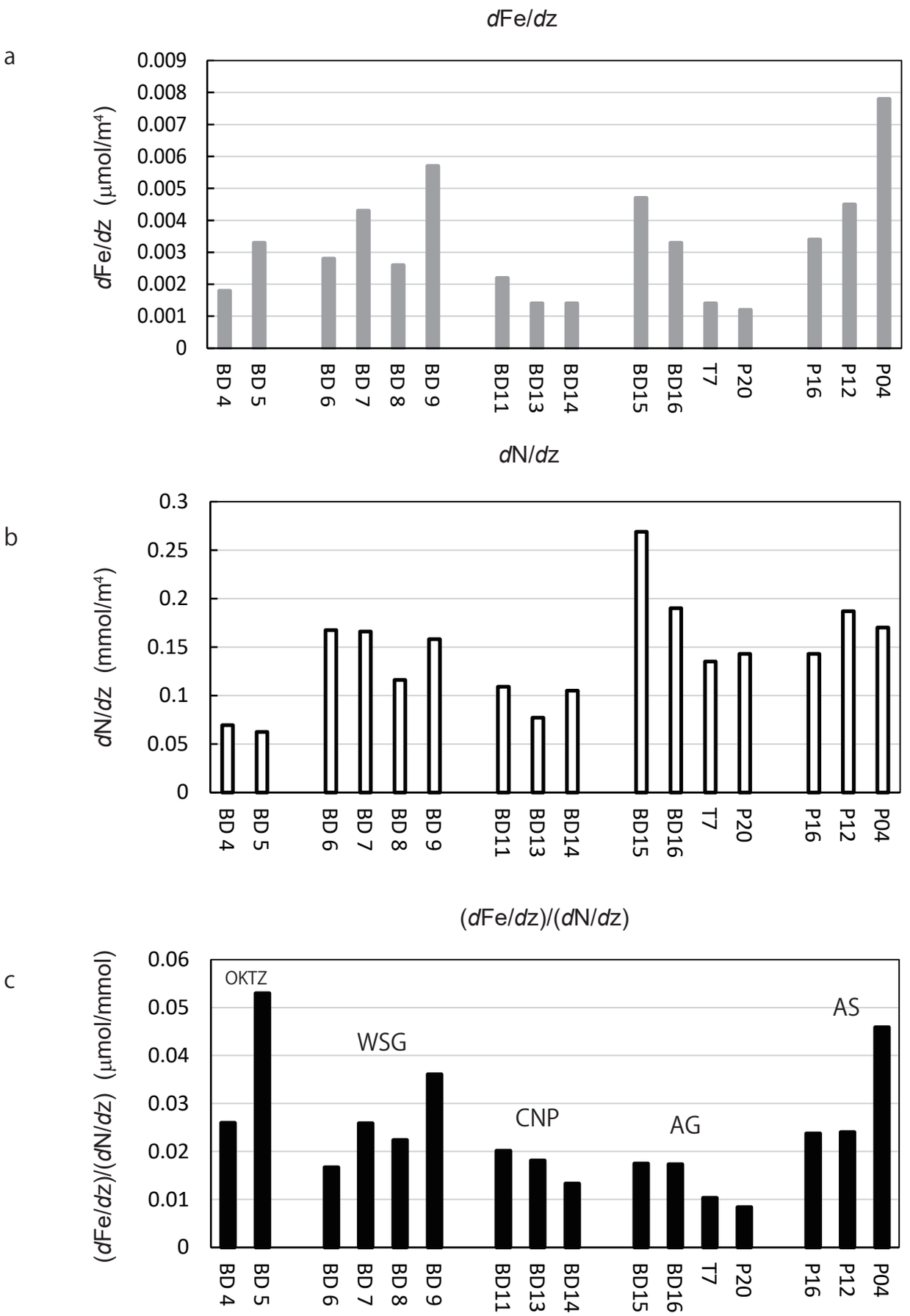


Figure 7

Dissolved Fe concentration/depth gradient (a), (*d*Fe/*dz*), nitrate+nitrite concentration/depth gradient (b), (*d*N/*dz*), and ratio of the dissolved Fe and nitrate+nitrite gradient (c), (*d*Fe/*dz*)/ (*d*N/*dz*), below surface mixed layer at stations BD 4, BD 5, BD 6, BD 7, BD 8, BD 9, BD11, BD13, BD14, BD15, BD16, and line P (OKTZ: Oyasio-Kuroshio Transition Zone, WSG: Western Subarctic Gyre, CNP: Central subarctic North Pacific, AG: Alaskan Gyre, AS: Alaskan Stream)

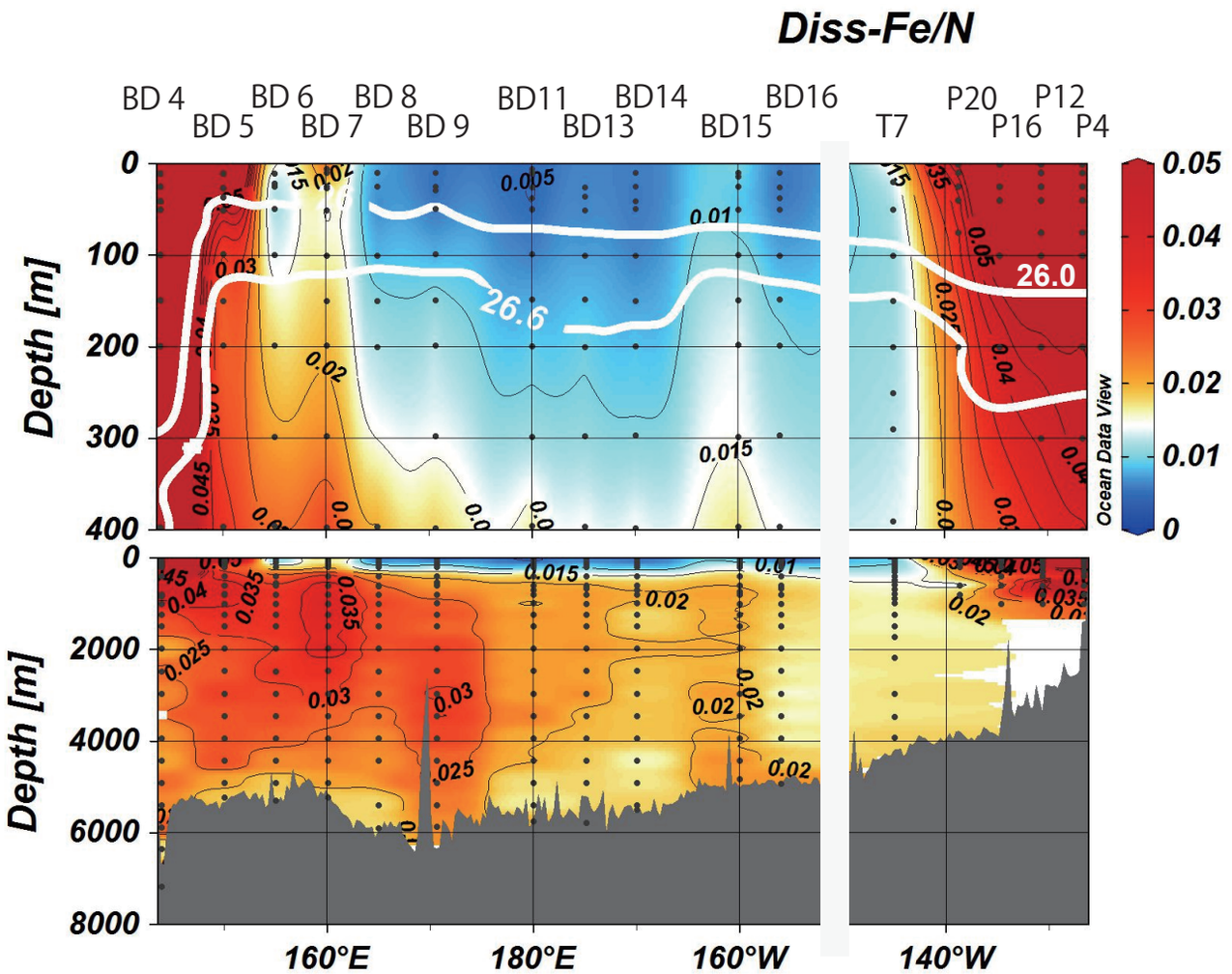


Figure 8

Vertical section profile of dissolved Fe and nitrate+nitrite concentration ratio including all stations from BD 4 to BD16, except BD 10 and BD 12, and line P (in Fig. 1) in the subarctic Pacific. The solid white lines in the figure indicate the 26 and 26.6 σ_θ isopycnal surfaces which are indicating bottom of winter mixed layer in the Alaskan Gyre (AG) and Oyasio-Kuroshio Transition Zone (OKTZ) + Western Subarctic Gyre (WSG), respectively. Upper panel shows 0 m to 400 m and lower panel show 0 m to bottom. Line P data is cited from Martin et al. 1989 and Nishioka et al. 2001. This figure is drawn using ODV (https://odv.awi.de/en/home/).

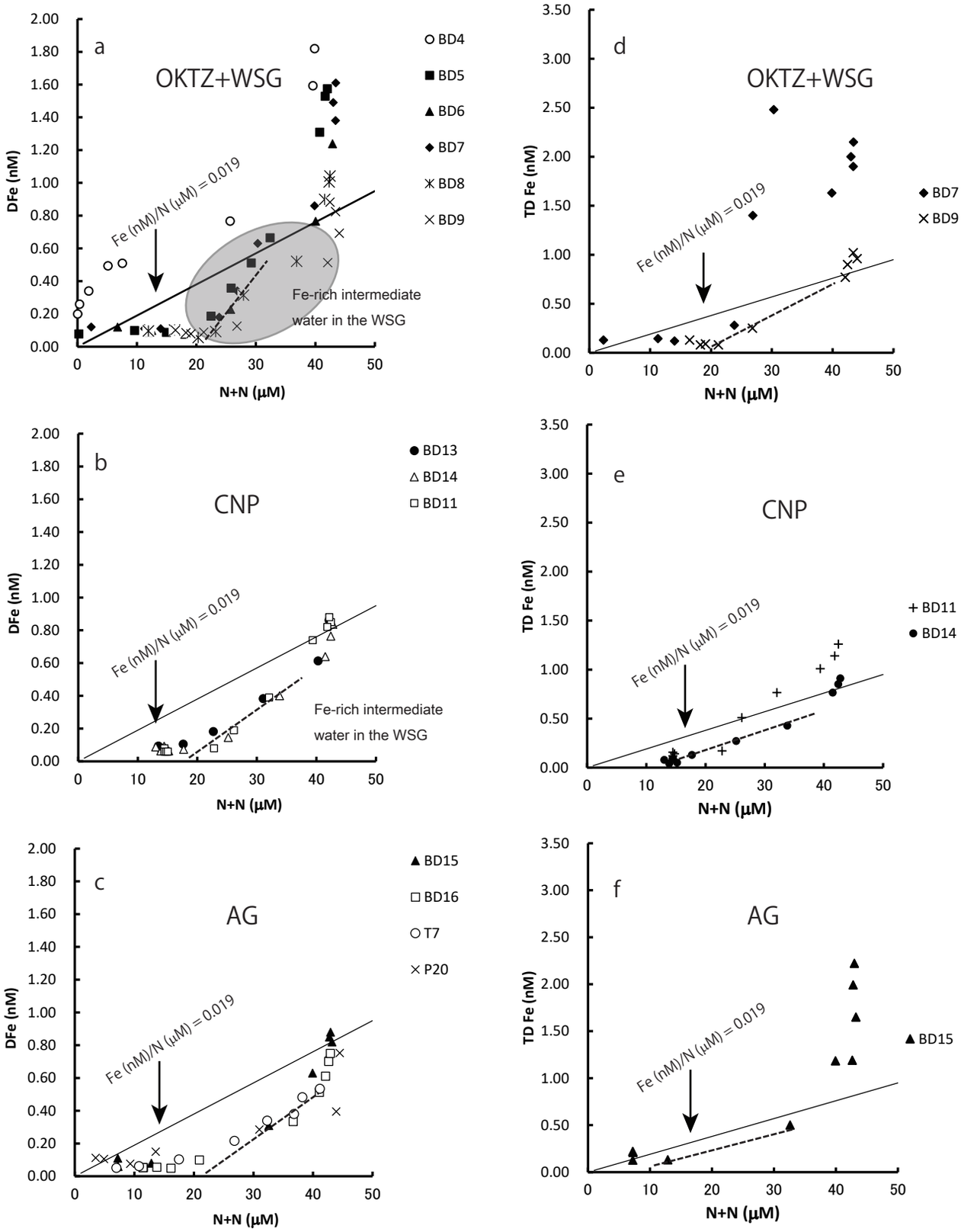
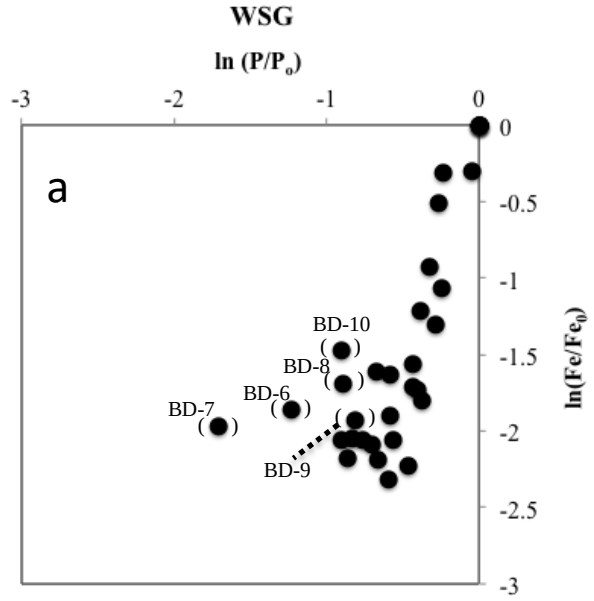


Figure 9

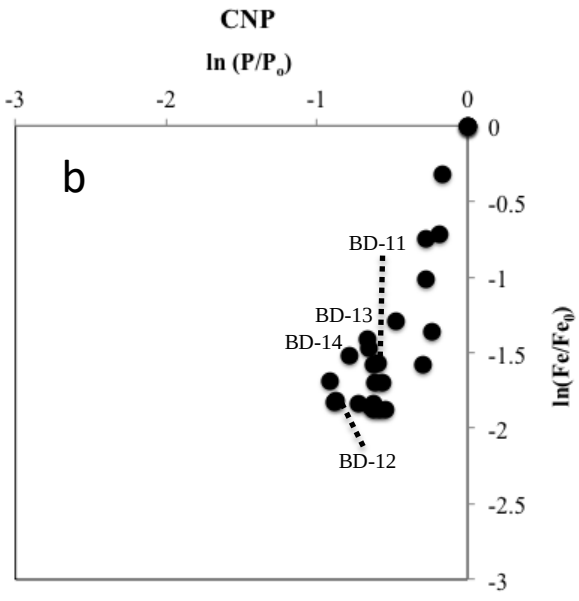
Comparison of sub-surface Fe to nitrate+nitrite (N+N) ratio with Fe and nutrient demand in surface diatom. Plots of dissolved Fe (DFe) versus N+N, (a) for data from the Oyashio-Kuroshio Transition Zone (OKTZ) and the Western Subarctic Gyre (OKTZ+WSG:BD 4, BD 5, BD 6, BD 7, BD 8, BD 9), (b) for data from Central North Pacific (CNP: BD 11, BD 13, BD 14) and (c) for data from Alaskan Gyre (AG: BD 15, BD 16, T7 (Martin et al. 1989), P20 (Nishioka et al., 2001). Plots of total dissolvable Fe (TDFe) versus nitrate+nitrite (N+N), (d) for data from WSG (BD 7, BD 9), (e) for CNP (BD 11, BD 14), and (f) for AG (BD 15). Solid line indicates Fe(nM)/N(μM) = 0.019, which is calculated by using reported minimum Fe demand (Marchetii et al. 2006). Dotted line indicates Fe(nM)/N(μM) increasing ratio in the water column from surface to intermediate waters.

WSG (BD-6-10)



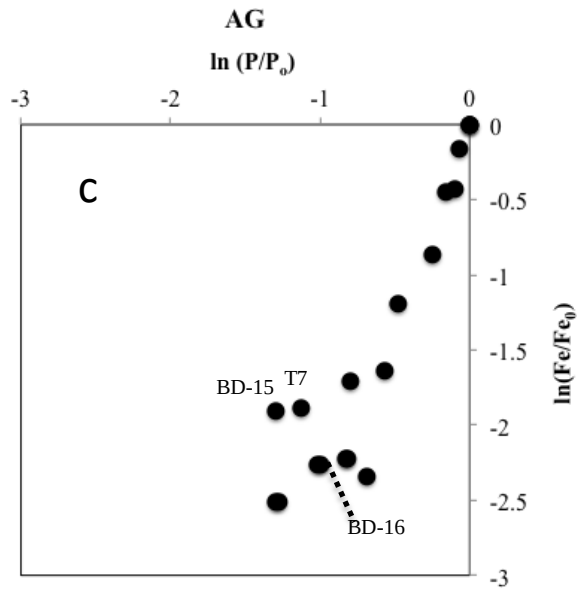
Slope: 3.01 ± 0.26
Without 10m: r^2 = 0.803
With 10m: r^2 = 0.373

CNP (BD-11-14)



Slope: 2.67 ± 0.29
Without 10m: r^2 = 0.764
With 10m: r^2 = 0.725

AG (BD-15, 16, T7)



Slope: 2.21 ± 0.21
Without 10m: r^2 = 0.764
With 10m: r^2 = 0.832

Figure 10

Evaluation of Fe and PO_4 fractionation in the upper 200 m. Plots of ln (P/P_0) vs ln(Fe/Fe_0) (a) in the Western Subarctic Gyre (WSG), (b) in the Central North Pacific (CNP), and (c) in the Alaskan Gyre (AG) in shallower than 200 m. P_0 and Fe_0 are initial concentrations in waters at 200 m deep. Plot in brackets (or indicated by dashed line) indicates the data at 10 m in each profile.

Table 1 Comparison of biogeochemical parameter between the Western Subarctic Gyre and the Alaskan Gyre

	Western subarctic Gyre		Alskan Gyre	references
Observed Chl.a maximum	0.5 - 1.5 mg/m3	>	0.3 - 0.6 mg/m^3	e.g. Boyd and Harrison, 1999 Boyd et al. 1995 Shiomoto et al. 1998 Imai et al., 2002 Harrison et al., 2004
Nitrate conc. (Winter maximum)	20 - 24 μM	>	15 - 17 μM	e.g. Tsurushima et al., 2002 Whitney and Freeland, 1999 Whitney, 2011 Chierici et al., 2006 Yasunaka et al., 2014
Nitrate conc. seasonal drawdown	15 - 20 μM		7 - 10 μM	e.g. Tsurushima et al., 2002 Whitney and Freeland, 1999 Whitney, 2011 Chierici et al., 2006 Yasunaka et al., 2014
*P*CO2 Biological Seasonal drawdown	higher	>	lower	e.g. Takahashi 2002 Chierici et al., 2006 Yasunaka et al., 2014
Organic C, Opal flux	higher	>	lower	Honda, 2003, Honda et al., 2002 Wong et al., 1999 Busseler et al., 2007
Dominant Phytoplankton	Diatoms		Diatoms	e.g. Mochizuki et al., 2002 Harrison et al., 2004
photochemical quantum yield (Fv/Fm)	higher	>	lower	Suzuki et al., 2002 Fujiki et al., 2014
Limiting factor for phytoplankton growth	Fe		Fe	e.g. Tsuda et al., 2003 Boyd et al., 2004